SLA

DE8

NEW RESULTS ON MESONS
CONTAINING STRANGE QUARKS[*]

D. Aston,[a] N. Awaji,[b] T. Bienz,[a] F. Bird,[a] J. D'Amore,[c] W. Dunwoodie,[a] R. Endorf,[c]

K. Fujii,[b‡] H. Hayashii,[b♭] S. Iwata,[b♯] W.B. Johnson,[a] R. Kajikawa,[b] P. Kunz,[a] D.W.G.S. Leith,[a]

L. Levinson,[a♮] T. Matsui,[b‡] B.T. Meadows,[c] A. Miyamoto,[b‡] M. Nussbaum,[c] H. Ozaki,[b] C.O. Pak,[b‡]

B.N. Ratcliff,[a**] D. Schultz,[a] S. Shapiro,[a] T. Shimomura,[b] P. K. Sinervo,[a†] A. Sugiyama,[b]

S. Suzuki,[b] G. Tarnopolsky,[a♯] T. Tauchi,[b‡] N. Toge,[a] K. Ukai,[d] A. Waite,[a♮♮] S. Williams[a♯♯]

[a] *Stanford Linear Accelerator Center, Stanford University, P. O. Box 4349, Stanford, California 94305*

[b] *Department of Physics, Nagoya University, Chikusa-ku, Nagoya 464, Japan*

[c] *University of Cincinnati, Cincinnati, Ohio 45221*

[d] *Institute for Nuclear Study, University of Tokyo, 3-2-1 Midori-cho, Tanashi-shi, Tokyo 188, Japan*

Presented at the SLAC Summer Institute on Particle Physics,
Stanford, California, July 28 - August 8, 1986

C-PUB--4202

7 008319

ABSTRACT

Recent results on strange and strangeonium mesons are presented. The data come from a high sensitivity study (4.1 ev/nb) of K^-p interactions at 11 GeV/c using the LASS spectrometer at SLAC. The complete leading orbitally-excited K^* series up through J^P 5 and a substantial number of the expected underlying states are observed decaying into $K \pi^+$, $\bar{K}^0_s\pi^+\pi^-$, and $K\eta$ final states, and new measurements are made of their masses, widths, and branching ratios. Production of strangeonium states via hypercharge exchange is observed into $K^0_s K^0_s$, $K^- K^+$, and $K^0_s K^+\pi^\mp$ final states. The leading orbitally-excited ϕ series through $J^P = 3^-$ is clearly seen and evidence is presented for additional high spin structure in the 2.2 GeV/c^2 region. No $f_2(1720)$ is observed. The $K^0_s K^\pm \pi^\mp$ spectrum is dominated by $1^+(K^*\bar{K} + \bar{K}^* K)$ production in the region below 1.6 GeV/c^2. These results are compared with data on the same systems produced by different production mechanisms.

2

1. Introduction

The spectroscopy of light quark mesons continues to be an important area of investigation in high energy physics. There is now a substantial amount of experimental activity in the intermediate mass region between 1 and 2 GeV/c², particularly from the colliding beam machines, and there is an awareness that these data are important in the search for exotic objects and in the testing of basic features of the $q\bar{q}$ interaction. Making a significant contribution to these studies via "old-fashioned" hadroproduction requires quite substantial improvements in the sensitivity of the data compared with the many earlier experiments, as well as very high quality data with good resolution and good acceptance over a wide variety of physics channels. Today, I will describe some recent results from the LASS collaboration which address several important issues in the strange and strangeonium meson systems.

2. The Experiment

The experiment I will be discussing was performed by a collaboration of physicists from two Japanese and two U.S. institutions using the LASS spectrometer facility[1] which is shown in Fig. 1. LASS has 4π geometrical acceptance with excellent angular and momentum resolution, full azimuthal symmetry, excellent particle identification, and a high rate triggering capability. It is situated in an RF-separated beam which delivers an 11 GeV/c K beam of high purity (typically a 70/1 or better K/π ratio before tagging by beam Čerenkov counters). It contains two large magnets filled with tracking detectors. The first magnet is

3

a superconducting solenoid with a 22.4 kG field parallel to the beam direction. This is followed by a 30 kG-m dipole magnet with a vertical field. The solenoid is effective in measuring the interaction products which have large production angles and relatively low momenta. High energy secondaries, which tend to stay close to the beam line, are not well measured in the solenoid, but pass through the dipole for measurement there. Particle identification is provided by a Čerenkov counter ($\check{C}_1$) and a time-of-flight hodoscope (TOF) which fill the exit aperture of the solenoid, and by a Čerenkov counter ($\check{C}_2$) at the exit end of the dipole spectrometer. In addition, the dE/dx ionization energy loss in the cylindrical proportional chambers which surround the target is measured to separate wide angle protons from π's in the $1/\beta^2$ region below 800 MeV/c

The trigger for this experiment requires two or more charged particles to exit the target. It is formed by cluster counting logic attached to a set of proportional chambers which conceptually form a box surrounding the target. The trigger is essentially σ_{tot}, except for the all neutral final states, and is quite clean. About 85% of all triggers are good physics events. For an experiment with such an open trigger, the sensitivity of about 4 ev/nb for the K beam incident, which will be discussed today, is very high. This leads to a processed data sample of about 115 million events, which leads in turn to one of the major difficulties in performing this experiment. The data analysis burden is very large, requiring the equivalent of about three IBM 3081/K years for completion. The task was shared between Nagoya University, utilizing a dedicated FACOM M200 at the High Energy Laboratory and the University Center's M382, and a nine processor 168/E farm at SLAC.

3. Motivation

Substantial progress in understanding the physics of meson systems has been made during the 10 year period following the "November Revolution" with the discovery of the heavy quarkonia, and their detailed study in the e^+e^- colliding machines. However, it remains clear that complementary studies of the light quark spectra are extremely important and provide access to important features of the spectroscopy which otherwise remain closed. First, as Fred Gilman discussed earlier in this school,[2] the light quark spectrum probes a different piece of the $q\bar{q}$ potential. In particular, the $c\bar{c}$ and $b\bar{b}$ systems probe the short range behavior of the potential while an excited light quark system, such as one that is spun up in orbital angular momentum, allows the study of the strength and Lorentz structure of the confining term.

Second, the hadroproduction mechanism is sufficiently different than production in colliding e^+e^- machines that the experimentally accessible excitations are nearly orthogonal. Figures 2 (a) and (b) are level diagrams (called Grotrian plots by nuclear physicists) which illustrate this for the $c\bar{c}$ and strange spectra respectively. The levels are arranged so that the states with quark spins antiparallel $(S = 0)$ are on the left, while states with quark spins parallel $(S = 1)$ are on the right. Orbital excitations appear as columns in each section which increase from $L = 0$ (S wave) on the left to $L = 3$ (F wave) on the right. Radial excitations appear as towers going up each of these columns. The positions at which the levels appear in mass should be considered as illustrative only for purposes of this discussion. The primary emphasis here is on the experimentally known excitations. In Fig. 2(a), the $c\bar{c}$ states which are included in the latest summary

table of the Particle Data Group[3] are shown. It should be noted that there are classification ambiguities in a few cases for the higher lying 1^- resonances, but the basic experimentally observed level structure is a very beautiful tower of 1^- radial excitations, with only the beginnings of the orbital towers building up. The reason for this is that the 1^- states are directly produced in e^+e^- collisions while the observation of higher orbital states requires decays from the produced 1^- states and therefore are much rarer and more difficult to observe. This may be contrasted with the situation in K^* spectroscopy as shown in Fig. 2(b). Once again the states shown are taken from the 1986 PDG summary tables. There are no candidate radial states. However, the first few levels of the orbital excitation ladders can be clearly seen, both in the $S = 0$ and the $S = 1$ sectors. So it is clear that the production area which is used in the study of a spectroscopy is of vital importance in determining the states, and the features of the spectrum, which can be observed. In particular, e^+e^- collisions are without peer in producing clear 1^- radial towers, but the less specific hadroproduction mechanism is essential to the study of the higher orbital excitations.

Third, the recent speculation that some of the states observed in the 1 to 2.2 GeV/c^2 mass region in e^+e^- production may be exotic objects such as "glueballs" points up once again the importance of understanding the ordinary $q\bar{q}$ states in this same mass region in order to understand whether any particular state is "unusual", and different production mechanisms may be crucial in this process. For example, the production of light mesons decaying to $K\overline{K}$ in K^-p interactions is dominated at small values of momentum transfer by hypercharge exchange processes (K and K^* exchange) and would be expected (and is known) to be

dominated by the production of strangeonia ($s\bar{s}$ mesons), while the production of the same final states via radiative decays from the J/ψ might be expected to contain a rather large admixture of glueballs. So the combination of these different production mechanisms should be very powerful in sorting out the nature of any new or unusual states which are observed.

4. The Strange Mesons

For a variety of reasons, the strange mesons appear to be an excellent place to try to understand a pure $q\bar{q}$ spectrum. First, flavored (i.e., K) beams are available which allow the strange mesons to be produced cleanly with large cross sections. Second, the charge-exchange channels are dominated by the well understood π exchange mechanism, which allows studies of $K\pi$ scattering via extrapolation, and a clear look at both orbital excitations and the underlying states. Third, neutral Ks are visible via the K^0_s decay, so that it is rather easy to study all charges of final states with the good resolution of tracking detectors rather than using a neutral detector such as a shower counter. Finally, the $q\bar{q}$ final states have overt flavor so that there is no isoscalar-isovector mixing and no confusion with glueballs. The reaction

$$K^- p \to K^- \pi^+ n \qquad (1)$$

is an ideal place to study the orbital excitation ladder. This final state is topologically simple, is restricted to only the natural spin-parity series, and has a large cross section which is dominated by π exchange at small values of momentum transfer ($t' = t - t_{min}$). Many features of this channel are illustrative of

7

the physics and analysis methods used throughout this talk, particularly in the strangeonium sector, so I would like to discuss some of these features in detail. The invariant mass for Reaction (1) is shown in Fig. 3 for all 730,000 events with $|t'| < 1.0$ $(GeV/c)^2$. The spin-parity $J^P = 1^- K^*(892)$ and $2^+ K_2^*(1430)$ mesons can be clearly seen as can a higher mass structure in the $3^- K_3^*(1780)$ region. However, even with the enormous statistics of this plot, there is little evidence for additional structure in the high mass region where additional higher spin resonances would be expected. There are several different reasons for this. Reaction (1) contains not only K^* resonances, but nucleon (N^* and Δ) resonances as well. The large total amount of nucleon resonances produced in Reaction (1) is clearly seen in the invariant $n\pi^+$ mass plot shown in Fig. 4. It reflects rather smoothly into the $K^-\pi^+$ invariant mass distribution, but much less smoothly into the angular structure. In this situation, the easiest thing to do is cut out this portion of the phase space. This can only be done if the statistics of the experiment are very high since such a cut puts holes into the acceptance which must be corrected. With the large statistics of this experiment, we remove the events with $n\pi^+$ masses below 1.7 GeV/c^2 from the subsequent analysis. The remaining sample, which is shown in the cross-hatched histogram of Fig. 3, contains 385,000 events. However, even with the elimination of the nucleon resonances, the structure observable in the plot is essentially unchanged. The fundamental reason for this is that the $K\pi$ elasticity drops as a function of mass, so that the visible cross section for a given K^* resonance to decay in this channel decreases with increasing mass; in addition, the level structure of the spectroscopy, as shown in Fig. 2, leads to a large number of overlapping resonances in the region above 2.0

GeV/c^2. These effects conspire to yield the featureless distribution (observed in Fig. 3) at high mass.

Nevertheless, a great deal of interesting structure is hidden in this plot, as becomes evident when we increase its dimensionality. Figure 5 is a scatter plot of $K\pi$ invariant mass against the cosine of the t-channel decay angle of the K in the $K\pi$ center of mass (θ_{GJ}). The $K^*(892)$ stands out as a clear band, while there are big bumps, at both forward and backward θ_{GJ}, which indicate the $K_2^*(1430)$. As we continue to higher $M_{K^-\pi^+}$, the structure becomes more complex. For example, the large bump around $\cos(\theta_{GJ}) = -0.5$ in the 1.8 GeV/c^2 region, and a corresponding hole in the backward region, are associated with the $K_3^*(1780)$; the prominent backward peak just above 2.0 GeV/c^2 turns out to be related to the $K_4^*(2060)$.

Many other complex features are apparent in this plot, but it is also apparent that the understanding of the nature of these structures requires a detailed angular analysis. Today, we will concentrate on the leading K^* states in this channel, and so will discuss only the simplest analysis of this type, which is a spherical harmonic moments analysis. We select the data for this analysis to emphasize the π exchange contribution by requiring $|t'| < 0.2$ (GeV/c)^2. For pure π exchange, only moments with $M = 0$ are allowed, and a resonance of spin J can appear in moments up to $L = 2J$. In general, the leading orbitally excited resonances are expected to be the lowest lying states of high spin so that they will dominate the highest moments required at a given mass. For example, Fig. 6 shows the even L, $M = 0$ moments required to describe the data in the mass region below 1.88 GeV/c^2. Moments are not used in a particular mass region if they are consistent

9

with zero there. The 1^- $K^*(892)$, 2^+ $K_2^*(1430)$, and 3^- $K_3^*(1780)$ are clearly seen in t_2^0, t_4^0, and t_6^0, respectively. Each state dominates the highest moment required in the relevant mass region, and also appears with lower prominence in moments with lower L. Breit-Wigner fits to the $L = 2J$ moment give new measurements of the masses and widths of these states, indicated in Table I.

Table I

The parameters for the 1^-, 2^+, and 3^- states from a fit to the leading moments. The indicated errors are statistical and systematic respectively.

Resonance	J^P	Mass(MeV/c^2)	Width(Mev/c^2)
$K^*(892)$	1^-	$897.0 \pm 0.7 \pm 0.7$	$49.9 \pm 1.7 \pm 0.8$
$K_2^*(1430)$	2^+	$1433.0 + 1.6 \pm 0.5$	$115.8 \pm 2.7 \pm 1.6$
$K_3^*(1780)$	3^-	$1778.1 \pm 6.4 \pm 1.3$	$185.9 \pm 23.3 \pm 12.3$

Having observed the leading K^* states that are rather well understood, let us now look at candidates for higher orbital excitations. Figure 7 shows the required moments with $L > 6$, $M = 0$, in the region above 1.8 GeV/c^2. Moments, not shown, with $L > 10$ are consistent with zero. The peaks in the t_8^0 and t_{10}^0 moments, and the interference structures in the t_7^0 and t_9^0 moments are naturally interpreted as confirming the $4^+ K_4^*(2060)$ and demonstrating the existence of a $5^- K^*$ around 2.38 GeV/c^2. However, the large errors on the moments make it difficult to determine the parameters of these resonances from the leading moments alone. The curves shown in Fig. 7 result from a simple fit to all 21 moments in this mass region with $L \leq 10$, $M \leq 1$. The high spin F, G, and H waves are parameterized as relativistic Breit-Wigner forms. Background terms

which are linear in both amplitude and phase are used for the lower spin waves and added to the F, G, and H wave terms as well. The smaller $M = 1$ moments are related to the $M = 0$ moments using a parametrisation of earlier energy independent PWA results. The significance of the spin 5 state in this model is about 5σ. The masses and widths are shown in Table II.[4]

Table II

The parameters for the 4^+ and 5^- states from a fit to all moments. The indicated errors are statistical and systematic respectively.

Resonance	J^P	Mass (MeV/c^2)	Width (Mev/c^2)
$K_4^*(2060)$	4^+	$2062 \pm 14 \pm 13$	$221 \pm 48 \pm 27$
$K_5^*(2380)$	5^-	$2382 \pm 14 \pm 19$	$178 \pm 37 \pm 32$

The reaction

$$K^- p \to \bar{K}_s^0 \pi^+ \pi^- n \tag{2}$$

is an important source of information on the inelastic decay modes of the K^*s, and makes possible the observation of states with unnatural spin-parity. The invariant mass distribution ($M_{K\pi\pi}$), shown in Fig. 8, appears to show the expected leading $K_2^*(1430)$ and $K_3^*(1780)$ resonances over a substantial background. However, an analysis of these data[5] with the SLAC-LBL three-body PWA program[6] reveals that over 2/3 of this spectrum is resonant. Moreover, the peaks around 1.45 and 1.8 GeV/c^2 contain not only the expected leading resonances, but other underlying states with comparable intensities.

Even though I will not discuss the model in detail, it may be useful to briefly

11

review the approach taken in the analysis, and the labeling of the resulting three-body partial wave amplitudes. The model describes the $K\pi\pi$ final state as a superposition of two-body states made up of isobars, which decay into two particles, and a bachelor particle. The isobars of importance in this analysis are the $K^*(892)$, $K_2^*(1430)$, $\rho(770)$; a three-body phase space term is also required. The labeling of the amplitude components of the final state is given by the series of quantum numbers $J^P M^\eta$ (isobar) L, as illustrated in Fig. 9, where J is the total spin and P is the parity of the final state combination; M is the magnetic substate; η approximates the naturality of the exchange in the t channel; (isobar) is the isobar state; and L is the relative orbital angular momentum between the isobar and bachelor meson.

Let us begin by looking at the decomposition of the cross section into its spin-parity contributions. Figure 10 shows the natural spin-parity part. The 2^+, 3^-, and 4^+ cross sections appear to contain the same leading K^* states we just described in the $K\pi$ channel at 1430, 1780, and 2060 MeV/c^2 respectively. There is also a substantial amount of structure in the 1^- wave around 1.4 and 1.8 GeV/c^2, and in the 2^+ wave around 2.0 GeV/c^2. In fact, as we will discuss below, a further decomposition of the 1^- amplitude into the different isobar partial waves shows that the structure is caused by two 1^- states, at $\sim$ 1420 MeV/c^2 and 1740 MeV/c^2, and that essentially the entire natural spin-parity sector is resonant. On the other hand, the unnatural spin-parity waves, shown in Fig. 11, are only partially resonant. There is a large structure near 1400 MeV/c^2 corresponding to the $K_1(1400)$, but the other waves are rather smooth and featureless. The parameters of the resonant states are estimated by fitting

the partial wave amplitudes to Breit-Wigner resonances plus simple background terms. In the natural spin-parity sector, on which we concentrate today, we do a simultaneous fit to both 1^- waves, plus the $2^+ K^* \pi$, $3^- K^* \pi$, and $3^- \rho K$, using the known behavior of the three leading resonances to constrain the relative phase behavior of the 1^- waves. The fit requires two 1^- resonances, one at approximately 1.42 GeV/c^2, and the other at approximately 1.74 GeV/c^2. In Fig. 12, the intensities and phases of the leading $2^+ K^* \pi$, $3^- K^* \pi$ and $3^- \rho K$ are shown, along with the results of the 5-wave model fit just discussed, while in Fig. 13, we show the model fit to the 1^- amplitudes. The masses and widths of the 1^- resonant states are indicated in Table III.

Table III

The parameters for the two underlying 1^- states from the 5 wave fit described in the text. The indicated errors are statistical and systematic respectively.

Coupling	Mass (MeV/c^2)	Width (MeV/c^2)
$K^* \pi$	$1420 \pm 7 \pm 10$	$240 \pm 18 \pm 12$
$K^* \pi$, ρK	$1735 \pm 10 \pm 20$	$423 \pm 18 \pm 30$

In order to understand the nature of these states, it is useful to consider two more pieces of information. First of all, in the $K^- \pi^+$ channel there is a large resonant state with an elasticity of around 0.35 in the 1.75 GeV/c^2 region. However, the elasticity in the 1.4 GeV/c^2 region is less than 0.1, indicating that the coupling of the lower state to the two-body channel is strongly suppressed.[7] This suppression is corroborated by the production characteristics of the three-body amplitudes as shown in Fig. 14. The $|t'|$ dependence of the 1^- amplitudes in

the 1.73 to 1.85 GeV/c^2 region, shown by the open circles, is quite steep as would be expected from π exchange, while the slope of the 1$^-$ amplitude in the 1.37 to 1.47 GeV/c^2 region, shown by the closed circles, is flatter as would be expected from B exchange, for example. It should be noted that the relative phase between the 1$^-$ state at $\sim$ 1420 MeV/c^2 and the $K_2^*(1430)$ is $\sim$ 90°, whereas the phase between the 1$^-$ state at $\sim$ 1735 MeV/c^2 and the $K_3^*(1780)$ is $\sim$ 0°. This is also indicative of a different production mechanism for the two 1$^-$ states.

This behavior leads naturally to our preferred classification of these two 1$^-$ states. Though mixing is not entirely excluded, it is simplest to associate the higher state with the 1^3D_1 state based on the small $L \cdot S$ splitting and the similarity of the widths and branching ratios with typical quark model calculations. The lower state then becomes mostly the first radial excitation of the $K^*(892)$. The suppression of the $K\pi$ decay mode of this lower state is understood in some models as being a dynamical effect resulting from the presence of a node in the radial wave function.

There is an additional new structure which can be seen in these three-body amplitudes. Figure 15 shows the behavior of the 2$^+$ amplitudes. In addition to the well-known leading $K_2^*(1430)$, a large structure is evident in the mass region around 2.0 GeV/c^2. We have fit these amplitudes in the region above 1.69 GeV/c^2 to a model which incorporates a Breit-Wigner resonance and a linear coherent background. The phase is essentially constrained by the leading 3$^-$ $K^*\pi$, as incorporated in the 5-wave fit described above. The fit, which is indicated by a solid line in Fig. 15, gives a mass of $\sim$ 1.97 GeV/c^2 with a width of $\sim$ 0.37 GeV/c^2. However, since a substantial background is required, the single resonance fit is

14

not unique. In fact, the data can be fit equally well in a two resonance model with the second resonance at a somewhat higher mass.

Figure 16 summarizes the states we have observed in the $\overline{K}^0_s \pi^+ \pi^-$ final state along with our preferred quark model assignments. The shaded regions correspond to the experimental errors on the mass values, while the stars indicate the mass values predicted by the model of Godfrey and Isgur.[8] The J-values of the leading states are linear in mass squared, and the $L \cdot S$ splitting appears to be quite small. In general, the model does rather well. The greatest difficulty is with the 1 radial state which is predicted to lie significantly above the observed state.

Other good testing grounds for mesonic models are their predictions for decay rates and branching ratios. In particular, the K^* mesons should decay into the $K\eta$ final state. However, the visible cross sections are expected to be rather small and the final state is difficult to study experimentally, so there is very little data available from earlier experiments. In the present experiment, we have looked at events which satisfy a 1C kinematic fit to the channel

$$K^- p \to K^- \pi^+ \pi^- \pi^0 p \quad . \tag{3}$$

Events which satisfy a 4C fit to $K^- \pi^+ \pi^- p$ are rejected. The resulting $\pi^+ \pi^- \pi^0$ mass spectrum is shown in Fig. 17. There is a large η signal over some background. The shaded regions serve as controls for background subtraction. Figure 18 shows the invariant $K^- \eta$ mass distribution after subtraction of the control regions and a set of cuts to remove the Y^* and N^* overlap. The spectrum is dominated by a single bump with a mass and width which are consistent with

the 3⁻ $K_3^*(1780)$ resonance. Preliminary results of the moments analysis also require substantial production of a spin 3 resonance. Assuming that $K_3^*(1780)$ dominates the region, the observed cross section corresponds to a branching ratio $K_3^*(1780) \to K\eta$ of ~ 2.5%. In contrast, there is no evidence at all for a decay of the $K_2^*(1430)$ to $K\eta$. The shaded area centered at 1.43 GeV/c² shows the signal expected for a $K_2^*(1430) \to K\eta$ branching ratio of 0.5%, which is clearly a conservative upper limit on the decay. Though the branching ratios for the 2⁺ and 3⁻ leading K^* resonances differ by at least a factor of five, the results of standard models[8] appear to agree at least qualitatively with this result.

Figure 19 summarizes the K^* spectrum observed to date in this experiment, most of which we have discussed today. The observed leading states in the orbital ladder now extend all the way through the 5⁻ K^*. Many of the expected underlying states have now been seen and there are good candidates for several radial states. We have seen π transitions from most of these states, as well as transitions to vector, and in some cases, tensor mesons. Rare decays into final states such as $K\eta$ are also beginning to be observed. The clear experimental picture now emerging provides powerful tests of existing $q\bar{q}$ models, and imposes important constraints on the predictions which might result from future modifications to them.

5. Strangeonium Mesons

The ability of the LASS spectrometer to reconstruct V^0 decays provides a very clean way to study the production of strangeonium mesons. In all cases discussed today, we will look only at fully constrained channels with a slow Λ recoil. Thus, the backgrounds are small; resolution is very good; particle identification requirements are minimized; and the resulting geometrical acceptance is nearly flat. As discussed earlier, the dominant production process in a K induced reaction at small t with a Λ recoil is hypercharge exchange. This leads us to expect very clean production of the strangeonia into channels containing a $K\overline{K}$ in the final state.

The $K\overline{K}$ invariant mass spectrum from the reaction

$$K^- p \rightarrow K^- K^+ \Lambda \tag{4}$$

shown by the open histogram in Fig. 20 confirms these expectations. The distribution is dominated at low mass by the production of the classic strangeonia, the $1^- \phi(1020)$ and the $2^+ f_2'(1520)$, while there is another smaller bump at 1.86 GeV/c^2, the $\phi_J(1850)$ to be discussed below, which is expected to be the next state on the strangeonium orbital ladder. In general, the $K^- K^+$ (strangeonium) invariant mass spectrum is very reminiscent of the $K^- \pi^+$ (strange) spectrum, Fig. 3, with an appropriate shift in the mass scale to account for the additional constituent s quark. This should be contrasted with production of the same final state with a π beam, as observed by the OMEGA spectrometer experiment of Evangelista et al.,[9] shown in the cross-hatched histogram of Fig. 20, where no

strangeness is exchanged. The bumps observed are associated with minority decay modes of objects without hidden strangeness, such as $f_2(1270)$, and $a_2(1320)$, interfering with strangeonium production.

Given that it is natural to expect strangeonium production in hypercharge exchange processes, the reactions

$$K^- p \to K^o_s K^\pm \pi^\mp \Lambda \qquad (5)$$

should be the ideal place to study the 1^+ strangeonium mesons which might be expected to lie in the 1.4 GeV/c^2 region, and for which evidence has been claimed in earlier experiments.[3,10] The invariant mass for the combined channels, shown in Fig. 21, has clear structure in the mass regions just above 1.5 GeV/c^2 and around 1.85 GeV/c^2, close to the positions expected for the leading 2^+ and 3^- $s\bar{s}$ states, but little activity in the region below 1.5 GeV/c^2 except for a sharp rise at K^*K threshold. However, the major features are so reminiscent of the strange three-body $\overline{K}^o_s \pi^+ \pi^-$ channel discussed earlier, which contained complicated structure in the peak regions, as to make us very cautious about associating these structures with any known states until the results of a full PWA are available.

In spite of a long history of confusion regarding the data in the 1.4–1.5 GeV/c^2 region, the classical "E" meson (now called the $f_1(1420)$) has generally been taken as the 1^{++} strangeonium state,[3] so the lack of any clear structure in these data in the 1.4 GeV/c^2 region is somewhat disappointing. Given the rather narrow (56 MeV/c^2) width of the $f_1(1420)$, it is worth looking at the low mass spectrum plotted in 20 MeV/c^2 bins, as given in Fig. 22, to investigate the K^*K threshold region in more detail. There appears to be a small amount of $f_1(1285)$ production

followed by a sharp rise to what may be a small peak just above $K^* K$ threshold. However, not only is this structure of limited statistical significance, but it lies some 10–20 MeV/c^2 below the accepted mass value for the $f_1(1420)$ meson. The clearest structure is the rise at threshold. Overall, the impression of the peaks in the low mass region is that they look rather similar to but somewhat weaker than those produced into the same final state with π beams, which is not what would be expected if they are states with dominant $s\bar{s}$ content.

These final states are dominated by the production of $(K^* \overline{K} + \overline{K}^* K)$ for all masses. In particular, for the mass region below 1.64 GeV/c^2, this can be seen very clearly in the Dalitz plot of Fig. 23. However, the amounts of K^* and $\overline{K}^*$ are substantially different, which implies that this region is not dominated by the production of a single resonance.

Preliminary results from the PWA analysis of these channels indicate more clearly the nature of the dominant structure around 1.52 GeV/c^2. The number of events required to perform a fit with the isobar model is rather large, which has forced us to use rather wider bins than we would prefer in this region. Figure 24 shows all the waves required to fit these data in the mass region below 1.76 GeV/c^2 summed over isobars. The total cross section is dominated by the unnatural spin-parity waves everywhere and in particular by the 1^+ wave below 1.7 GeV/c^2. The peak at 1.52 GeV/c^2 is 1^+ and so does not correspond to the $(K^* \overline{K} + \overline{K}^* K)$ decay mode of the $f'_2(1520)$. In fact, this is as expected both in SU(3) and other more modern models[8] and results from the small amount of phase space and the large spin inhibition factor of this decay.

The 1^+ waves are all K^* isobars while the 0^- wave is a δ isobar. We find

19

no evidence for $0^- \delta \pi$ anywhere, although we cannot totally exclude a small production cross section around 1.42 GeV/c^2. The 1^+ K^* waves form a large bump centered at about 1.52 GeV/c^2 with a width of around 100 MeV/c^2, which it is tempting to ascribe to a "D' (1530)" [f_1(1520)] resonance previously claimed by Gavillet et al.[11] However, since the 1^+ wave dominates this region so completely, we are unable to make a convincing case for resonant phase motion. Moreover, the unequal production of K^* and $\overline{K}^*$ requires a more complex explanation than a simple one-resonance model. An attempt to better understand these data and their interpretation is in progress.

Not only do the $K\overline{K}\Lambda$ final states in Reaction (4) and the reaction

$$K^- p \rightarrow K_s^0 K_s^0 \Lambda \qquad (6)$$

provide a look at the hadroproduction of strangeonia, but they also can provide revealing comparisons with the $K\overline{K}$ spectra produced in radiative J/ψ decay, which might be expected to be glue-enriched. Reaction (4) couples to all natural spin-parity states, while Reaction (6) is restricted to the even spin states only. After restricting the data to events with $|t'| \lesssim 2.0$ (GeV/c)^2, both channels are very clean and the normalization agrees well between them in the f_2'(1520) region. The $K\overline{K}$ invariant masses shown in Fig. 25 contain the expected leading $1^- \phi$(1020), seen only in the $K^- K^+$ channel, as well as the f_2'(1520) in both channels. There is also evidence for a third leading orbitally excited strangeonium state, the ϕ_3(1850), which we will discuss below. The primary difference between the spectra, apart from the restriction to only even spin in the $K_s^0 K_s^0$, is what appears to be a large continuum in the high invariant mass region of

20

the $K^- K^+$ spectrum. This background results from the diffractive production of $N^* \to K^+ \Lambda$, as is clear from the Dalitz plot of Fig. 26. On the other hand, N^* production in the $K_s^0 K_s^0$ channel is small. The N^* background in the $K^- K^+$ channel becomes dominant in the region above 2.0 GeV/c^2, and reduces the effective sensitivity of the $K^- K^+$ channel compared to $K_s^0 K_s^0$ even though the visible cross section of the $K^- K^+$ is much larger.

In order to understand the high mass structures in the $K^- K^+$ data, we repeat the moments analysis technique described earlier for the $K^- \pi^+$ channel. The resulting moments distributions are shown in Fig. 27. The acceptance corrected mass spectrum , t_0^0, shows a clear peak around 1.86 GeV/c^2 and similar structures appear in all moments up to t_6^0. These structures confirm the existence of a $J^P = 3^-$ ϕ-like object in this mass region. Breit-Wigner fits, shown for t_0^0 and t_6^0, provide estimates of the parameters of this resonance. The t_6^0 moment is assumed to be dominated by the pure resonance while the t_0^0 moment is given a simple linear background. The fits to the t_0^0 give a mass of 1854 ± 9 Mev/c^2 with a width of 64 ± 21 MeV/c^2 while the fit to the t_6^0 moment gives consistent values of 1885 ± 26 and 86 ± 30 MeV/c^2, respectively. Preliminary results from the amplitude analysis confirm this result.

An object which has been observed in the mass region around 1.7 GeV/c^2 in the radiative J/ψ decays is the "θ" $[f_2(17?0)]$. It has a spin-parity 2^+ and is about 150 MeV wide.[10] Since it has even spin, it should be seen most conspicuously in hadroproduction in the $K_s^0 K_s^0$ channel. There are two decay modes which have been observed with approximately equal strength (the $K\overline{K}$ and the $\eta\eta$). There are a few (weak) claims for other decay modes but it appears to be

21

at least reasonable from the J/ψ decay data to guess that the partial width of "θ" going to $K\overline{K}$ is around 75 MeV, substantially larger than the $f_2'(1520)$ to $K\overline{K}$ partial width. Figure 28 compares the $K_s^0 K_s^0$ hadroproduction data with the radiative J/ψ data from the MARK III experiment.[12] The data from LASS have been multiplied by 0.127 to normalize the $f_2'(1520)$ peaks in the two experiments. There is clearly no evidence at all for production of a $f_2(1720)$ in LASS. It appears to be suppressed by at least an order of magnitude compared to $f_2'(1520)$ production, unlike the production via radiative J/ψ. This would appear to require either that there are some large $f_2(1720)$ decay modes waiting to be discovered, and   at there is a mechanism for suppressing simple decay modes like $\pi\pi$', or that the exchange mechanism is very different than for the nearby $f_2'(1520)$. Either way, the implication is rather strong that the $f_2(172J)$ is not a conventional strangeonium object in spite of its strong $K\overline{K}$ decay mode.

In contrast, data from this experiment and the MARK III do appear to be consistent in the high mass region around 2.2 GeV/c^2 where a narrow $X(2220)$ [called the $\xi(2220)$] has been claimed. Figure 29 compares $K_s^0 K_s^0$ mass distributions for the two experiments in the mass region between 1.8 and 2.7 GeV/c^2. The data are normalized to have the same number of total events in this mass interval which leads to multiplying the acceptance corrected LASS data by 0.42. The data are clearly compatible. While the statistics of this channel are too limited to perform a definitive spin-parity analysis, it is clear that the events are not distributed isotropically in the t-channel helicity frame. Figure 30 shows the $K_s^0 K_s^0$ spectrum for events in the forward region where $\cos\theta_{GJ} > 0.85$. The cut enhances the 2.2 GeV/c^2 region. Equivalently, the inset to Fig. 30 shows

22

that the t_3^0 and t_4^0 moments also have structure at 2.2 GeV/c². Though higher
moments are consistent with zero, this may simply result from a lack of statis-
tics. All in all, the data from this channel appear to confirm the MARK III
result that a rather narrow object whose spin is at least two exists at 2.2 GeV/c².
The K^-K^+ channels are not so directly comparable because of the large N^*
diffractive background in the LASS experiment which produces a background
underneath the strangeonium production. However, this background should be
smooth in K^-K^+ mass, and even though it leads to substantial moments up
to t_6^0, it should not cause any structure in them. The K^-K^+ moments shown
in Fig. 27, do show structure in the 2.2 GeV/c² region in all moments up to t_8^0.
Although not statistically compelling, this is most simply interpreted as evidence
for a spin 4 object at the same mass. Taking these results together, the simplest
interpretation appears to be that we are seeing evidence for the production of
the $L = 3$ strangeonium triplet expected to lie in this mass region on the basis
of quark models.[8]

6. Conclusions

The variety of topics addressed today indicates that there remains a great
deal of important physics to be learned in the light quark sector, provided that
the data are of sufficient quality and sensitivity. The strange mesons provide
a clear avenue to a spectroscopy of pure $q\bar{q}$ states, and good progress has been
made in understanding where the states lie and their decay modes. There are
now good candidates for most of the underlying states expected in the region
below 2.0 GeV/c², and the complete leading orbitally excited K^* series up to a

$J^P = 5^-$ at 2380 MeV/c^2 has been observed. Moreover, most of these states have been demonstrated to decay into more than one final state, and rare decay modes, such as the $K\eta$ decay of the $K_3^*(1780)$, have been seen. The QCD based spectroscopy models are successful in explaining the broad outlines of the strange spectrum, but they do have some difficulty in explaining the detailed behavior. For example, the 1^- $K^*(1410)$ state is most naturally explained as the first radial excitation of the $K^*(892)$, but it lies too low in mass to be easily explained by most of the models.

The "strangeonium" states produced in hypercharge exchange provide an important alternative window into the search for unusual states, such as glueballs, as well as a direct approach to the $s\bar{s}$ spectrum. Detailed comparisons of the states observed here with those observed in e^+e^- collisions are of particular value in attempts to elucidate their composition. The $K_s^0 K^\pm \pi^\mp$ final state gives evidence for weak $f_1(1285)$ production and perhaps even some evidence for narrow structure in the "E" $[f_1(1420)]$ region. However, the production seems very small for an $s\bar{s}$ resonance. The largest structure around is a $1^+ (K^* \overline{K} + K^* \overline{K})$ bump at 1.52 GeV/c^2, but it is difficult to prove it is resonant since the amount of K^* and $\overline{K}^*$ production in the region is very different. The $K\overline{K}$ final states clearly show the expected leading $s\bar{s}$ series up to a $J^P = 3^-$ state at 1860 MeV. Data in the high mass "$\xi(2220)$" $[X(2220)]$ region look remarkably like those from MARK III, and provide evidence for structure whose spin is at least 2^+ (and perhaps 4^+), as would be expected in a quark model. On the other hand, the data are completely different from the MARK III data in the region of the "θ" $[f_2(1720)]$, which raises interesting questions about the nature of the object

which has been seen in e^+e^- collisions.

References

1. D. Aston et al., The LASS Spectrometer, SLAC-REP-298 (1986).

2. F. Gilman, Proceedings of the SLAC Summer Institute on Particle Physics, 1986.

3. Particle Data Group, Phys. Lett, 170B (1986).

4. D. Aston et al., Phys. Lett. 180B, 308 (1986).

5. D. Aston et al., SLAC-PUB-3972 (1986).

   P. K Sinervo (Ph D. Thesis), SLAC-REP-299 (1986).

6 D. Aston et al . Sl AC-REP-286 (1985).

7. D. Aston et al, Phys. Lett. B100, 235 (1981).

8. S. Godfrey and N. Isgur, Phys. Rev. D32, 189 (1985), and Godfrey, private communication (1986).

9. C. Evangelista et al., Nucl. Phys. B154, 381 (1979).

10. S. Cooper Plenary talk at the XXIII International Conference on High Energy Physics, Berkeley, CA (1986).

11. P. Gavillet et al., Z. Phys. C16, 119 (1982).

12. R. M. Baltrusaitis et al., Phys. Rev. Lett. 56, 107 (1986).

Superconducting Coils
and Vacuum Vessel

Iron

Dipole Magnet

BEAM

Č

Č

LH$_2$ Target
Č Cerenkov Counter
Proportional Chamber
Magnetostrictive Chamber
Scintillation Counter Hodoscope

1 m

1 m
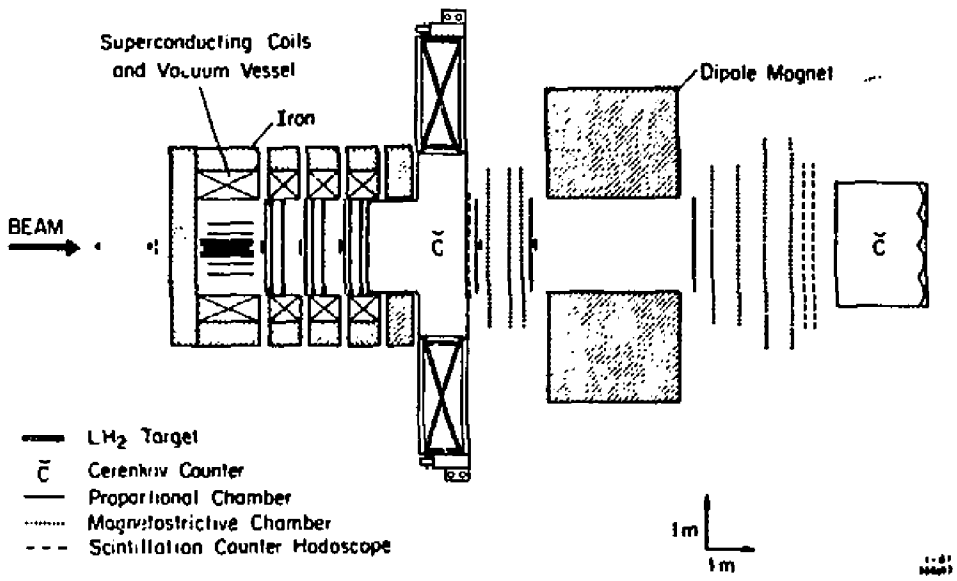
FIG. 1. The LASS spectrometer.
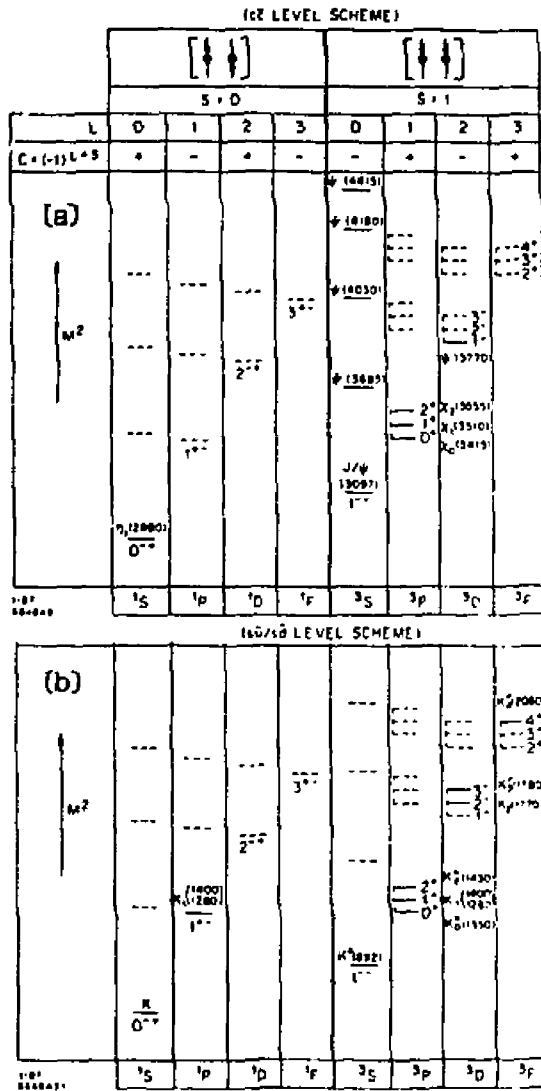
FIG. 2. Level diagrams for $q\bar{q}$ meson systems summarized in PDG tables: a) for charmonium states; b) for strange meson states. Mass levels are illustrative only and classification ambiguities, if any, have been neglected.
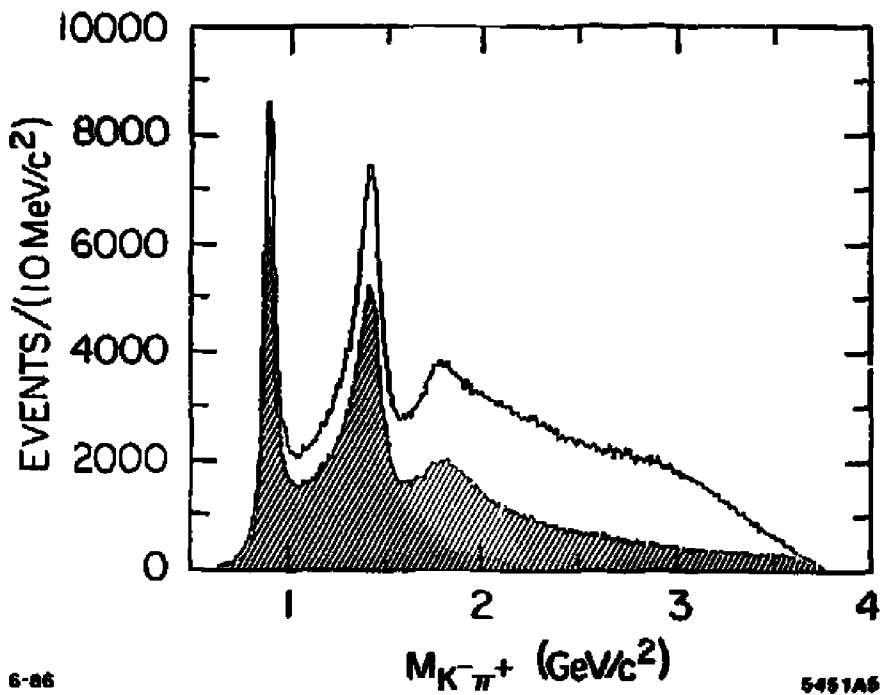
FIG. 3. The invariant $K^-\pi^+$ mass for the reaction $K^-p \to K^-\pi^+n$; the unshaded curve contains all events while the cross-hatched curve contains events with N^*'s removed (see text).
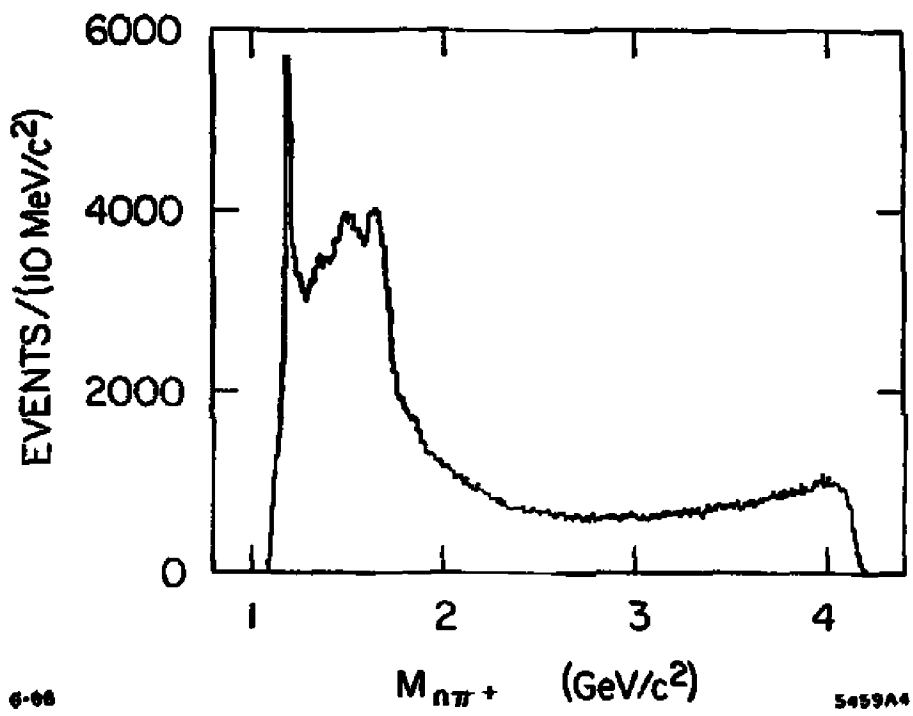
FIG. 4. The invariant $n\pi^+$ mass for the reaction $K^-p \rightarrow K^-\pi^+n$.
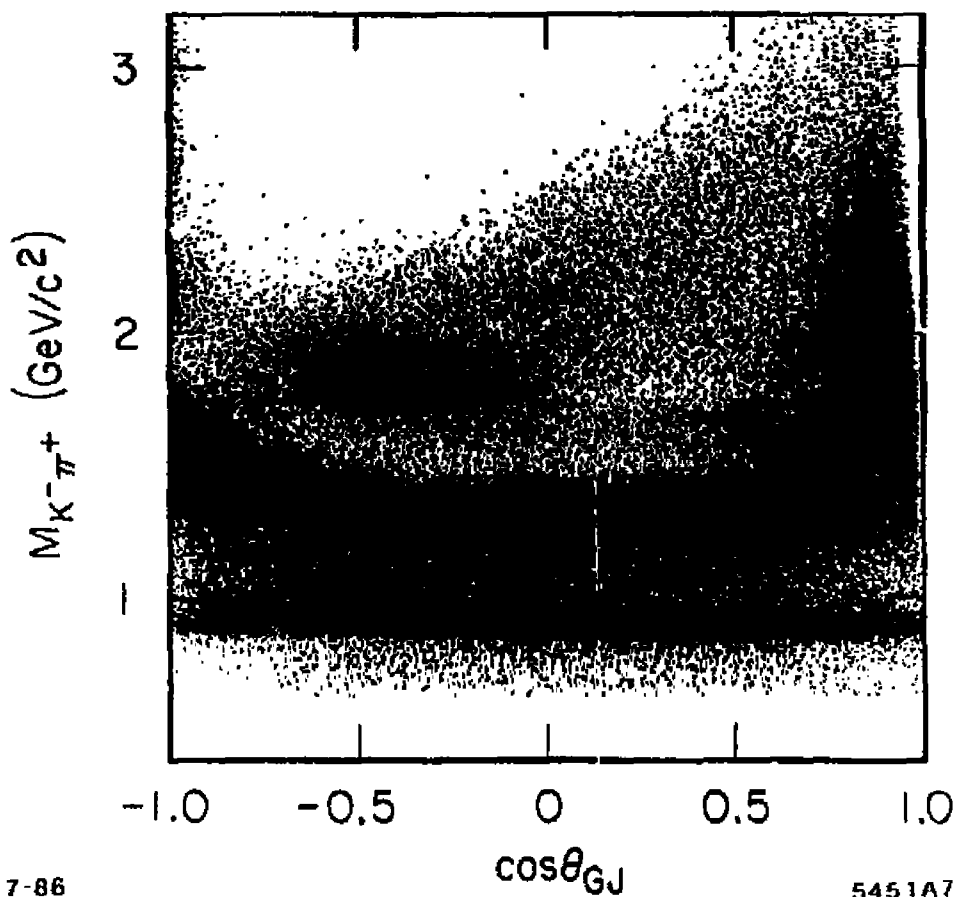
FIG. 5. The $\cos\theta_{GJ}$ vs. $M_{K\pi}$ scatter plot for events with $|t'| \le 0.2$ $(GeV/c)^2$; events near $\cos\theta_{GJ} = +1$ at high mass are removed by the N^* cut and by the removal of $K^- p$ elastic scattering.

51
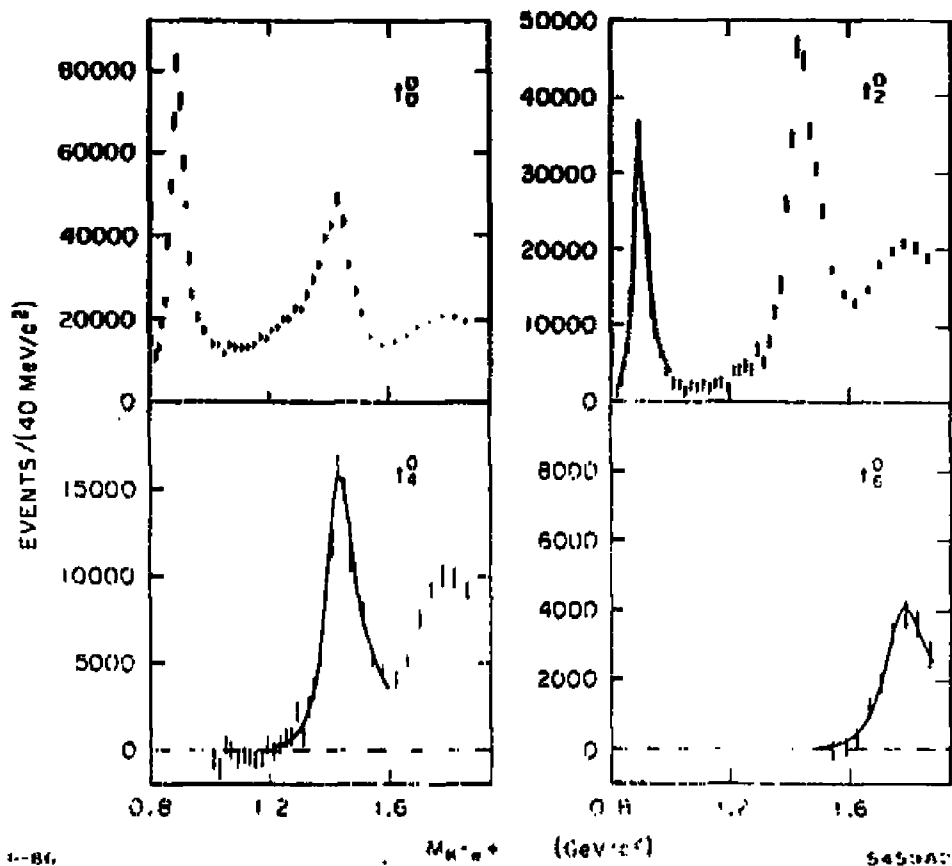
FIG. 6. The unnormalized L-even, $M = 0$ $K^-\pi^+$ moments for the mass region below 1.88 GeV/c^2; bin sizes vary from 10 to 40 MeV/c^2, with events normalized to 40 MeV/c^2 bins. The curves are described in the text.
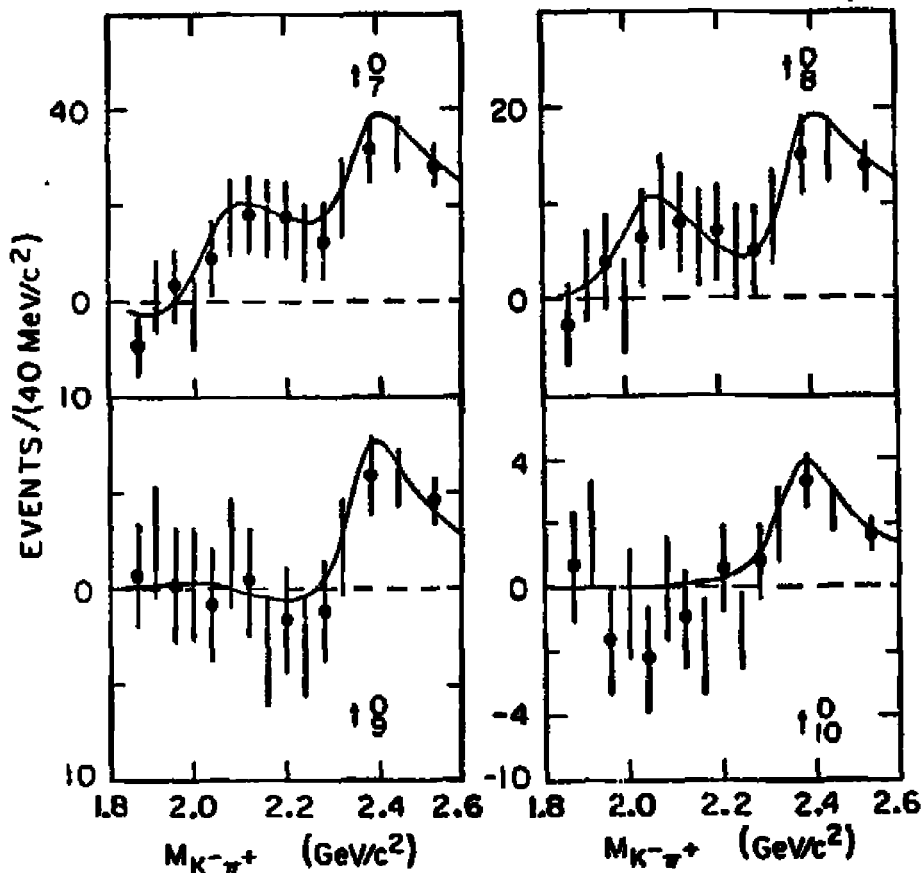
FIG. 7. The unnormalized $7 \leq L \leq 10$, $M = 0$ $K^-\pi^+$ moments for the mass region above 1.88 GeV/c^2. Moments with $L > 10$ are consistent with zero. The moments are plotted for overlapping bins; black dots indicate the independent set of mass bins used for the fit described in the text.
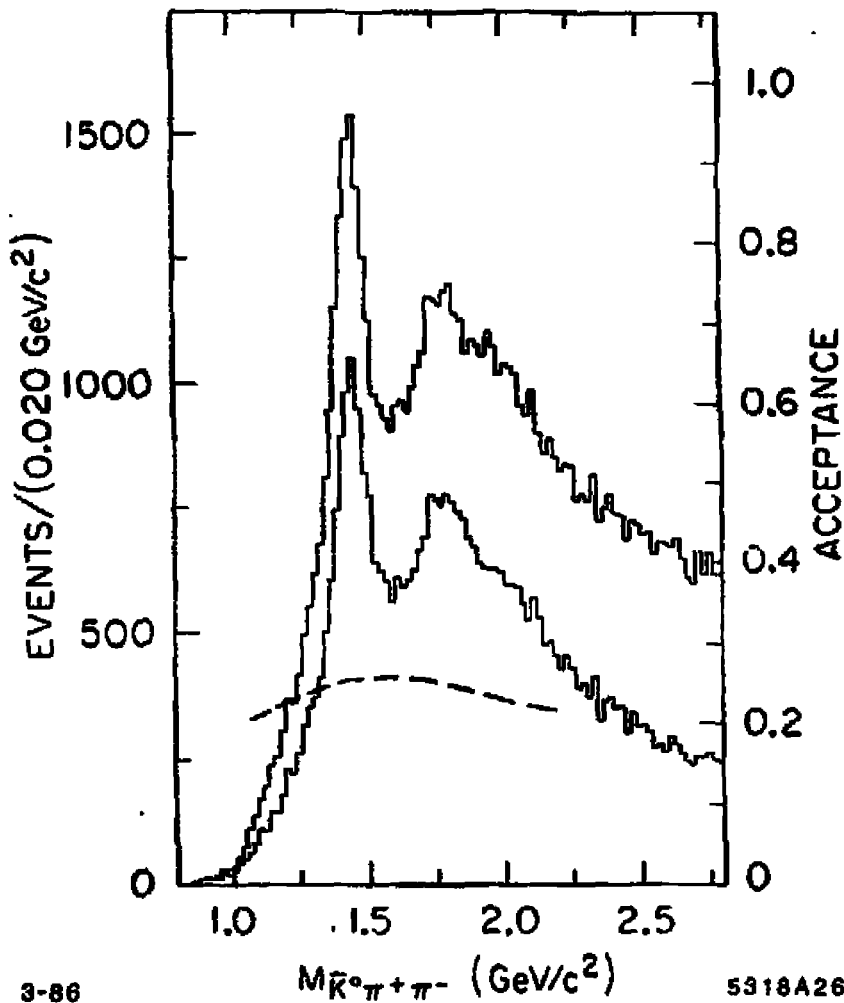
FIG. 8. The $\bar{K}^0_s\pi^+\pi^-$ invariant mass distribution. The outer histogram is for all events while the inner histogram contains only events with $|t'| \leq 0.3$ (GeV/c)^2. The dashed line gives the final acceptance after all cuts.
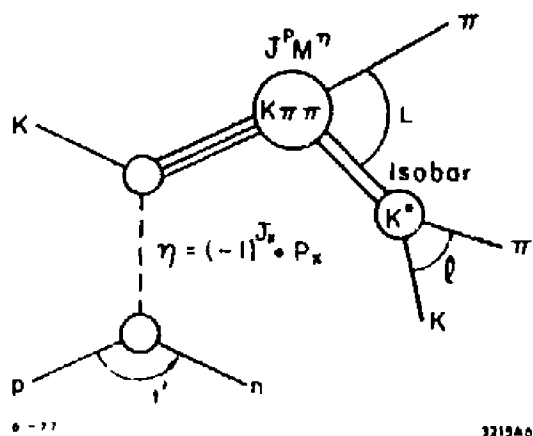
FIG. 9   Schematic diagram for $K \to K\pi\pi$ production describing the variables used by the isobar model.
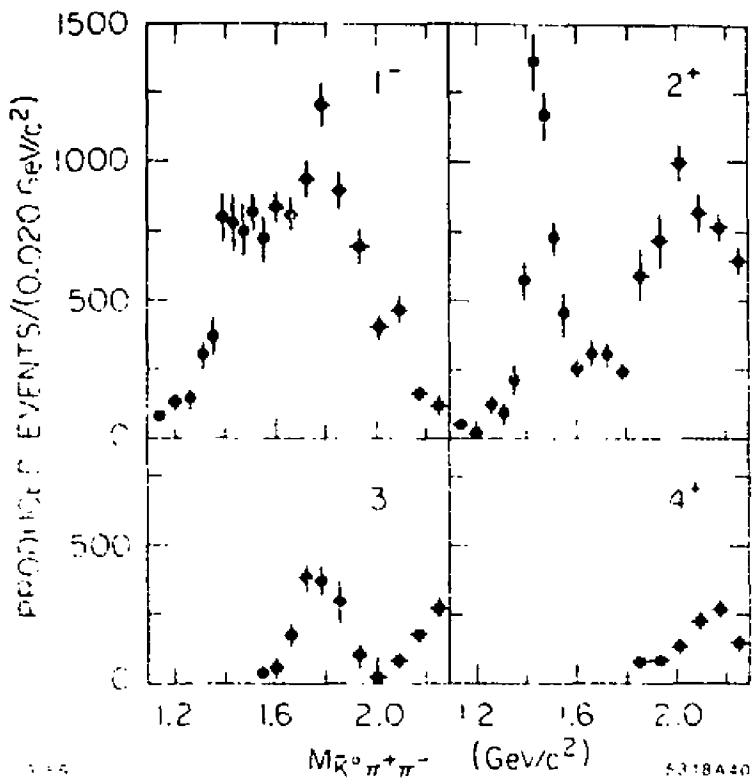
FIG. 10. The natural spin-parity wave sums for the $\bar{K}^0 \pi^+ \pi^-$ final states. All partial waves of the same J^P are summed coherently.
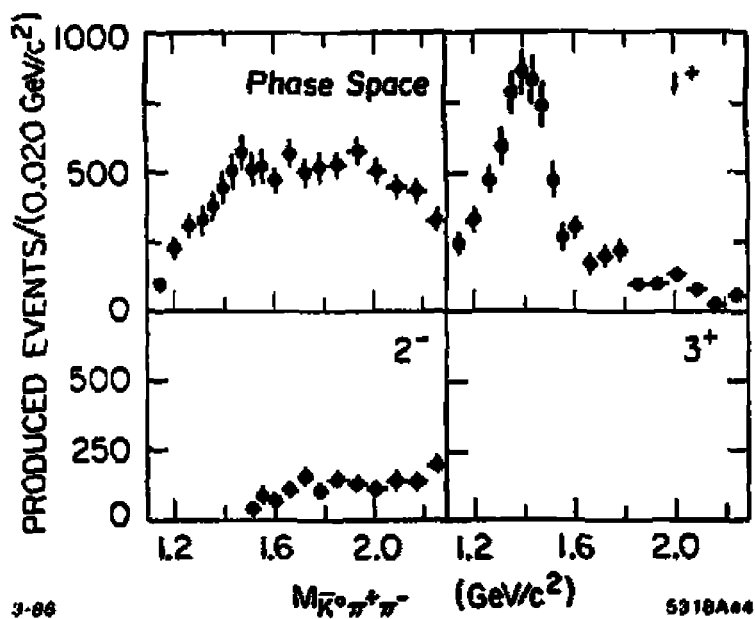
FIG. 11. The unnatural spin-parity wave sums for the $\bar{K}^0\pi^+\pi^-$ final state. All partial waves of the same J^P are summed coherently.
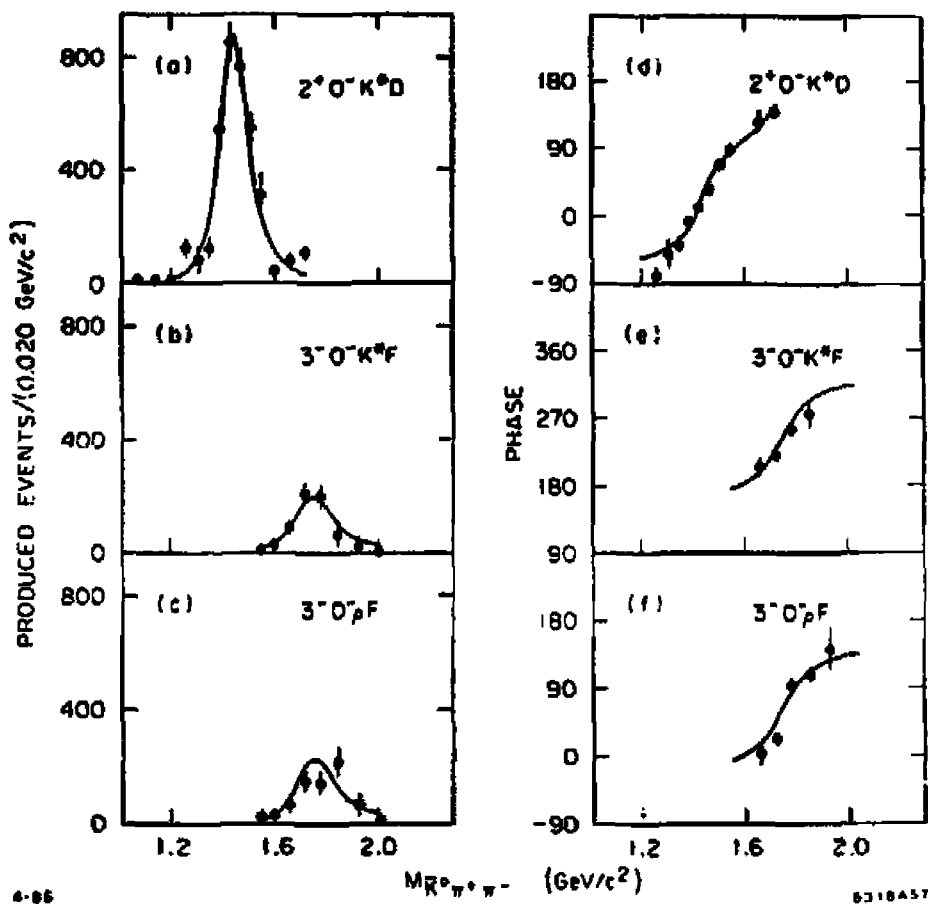
FIG. 12. The leading 2^+ and 3^- K^* resonant waves observed in $\bar{K}^0\pi^+\pi^-$, compared with the predictions of the 5 wave model discussed in the text.
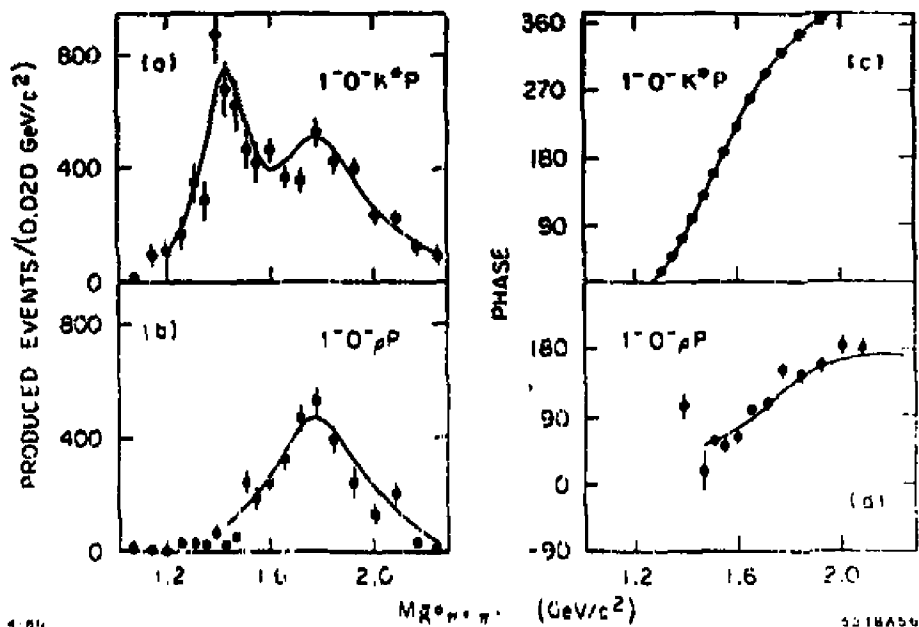
FIG. 13. The $\bar{K}^0\pi^+\pi^-$ 1⁻ waves compared with the predictions of the 5 wave model discussed in the text.
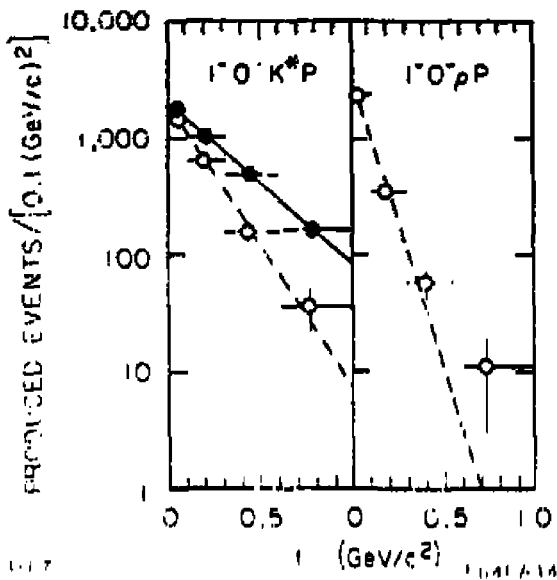
FIG. 14. The |t'| dependencies of the 1⁻ partial waves. The solid dots and line
are for the 1.42 GeV/c² mass bin. The open dots and dashed lines are for the
1.79 GeV/c² mass bin. The partial waves are modeled by a curve of the form $e^{bt'}$.
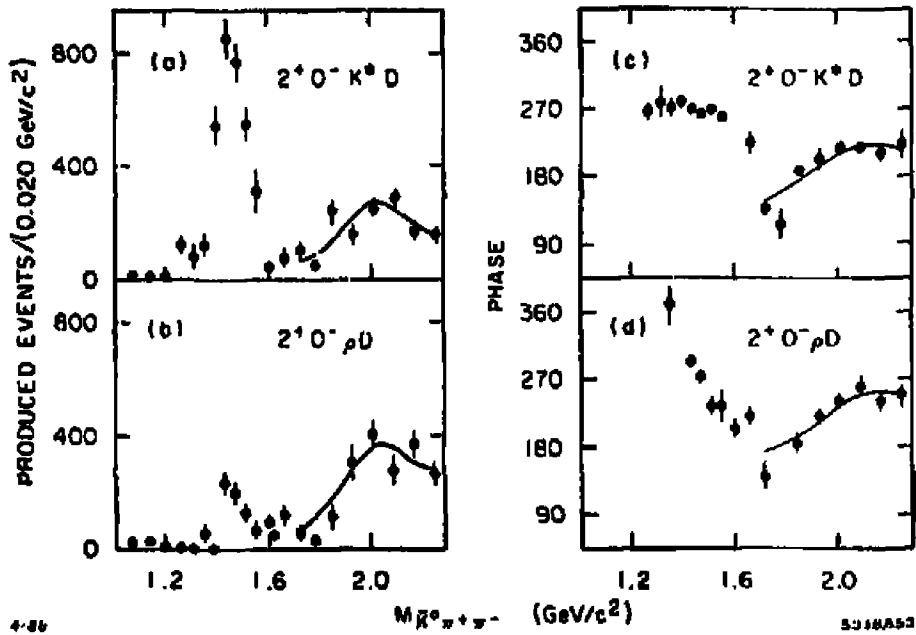
FIG. 15. The high mass $\bar{K}^0\pi^+\pi^-$ 2^+ waves. The solid line represents the fit to the high mass region described in the text.
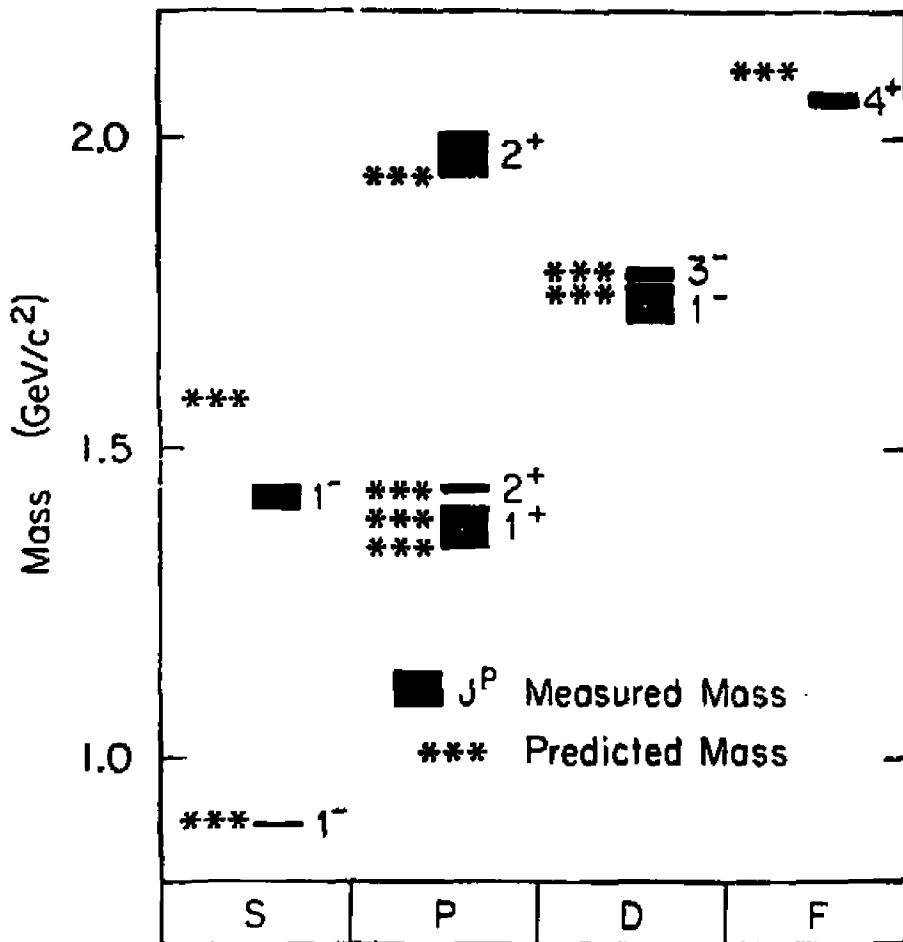
FIG. 16. Level diagram for the resonant $\bar{K}^{o}\pi^{+}\pi^{-}$ amplitudes observed in this experiment. The shaded regions indicate the measured uncertainty in the mass position. The predicted masses are taken from Ref. 8.
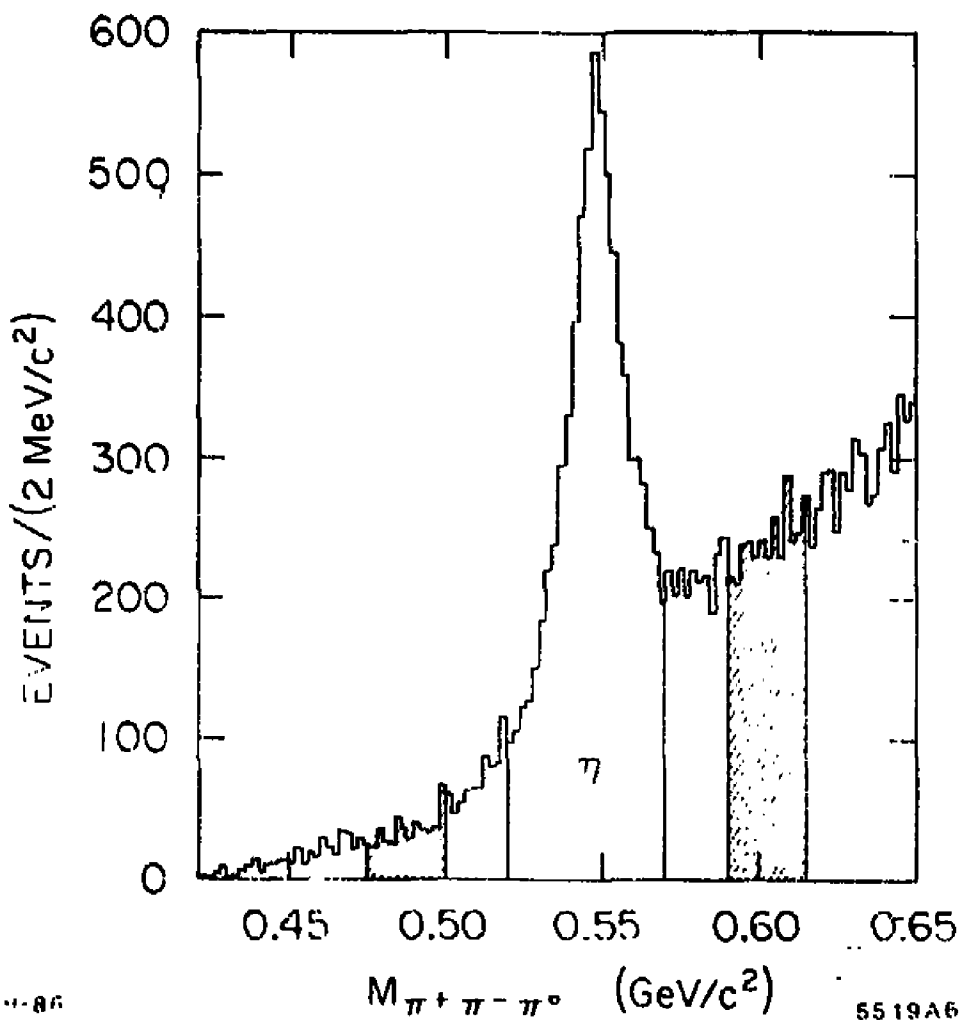
FIG. 17. The $\pi^+\pi^-\pi^0$ invariant mass from the reaction $K^-p \to K^-\pi^+\pi^-\pi^0 p$. The vertical lines indicate the region used to define the η signal. The shaded regions are used to estimate the background under the $K\eta$ signal.
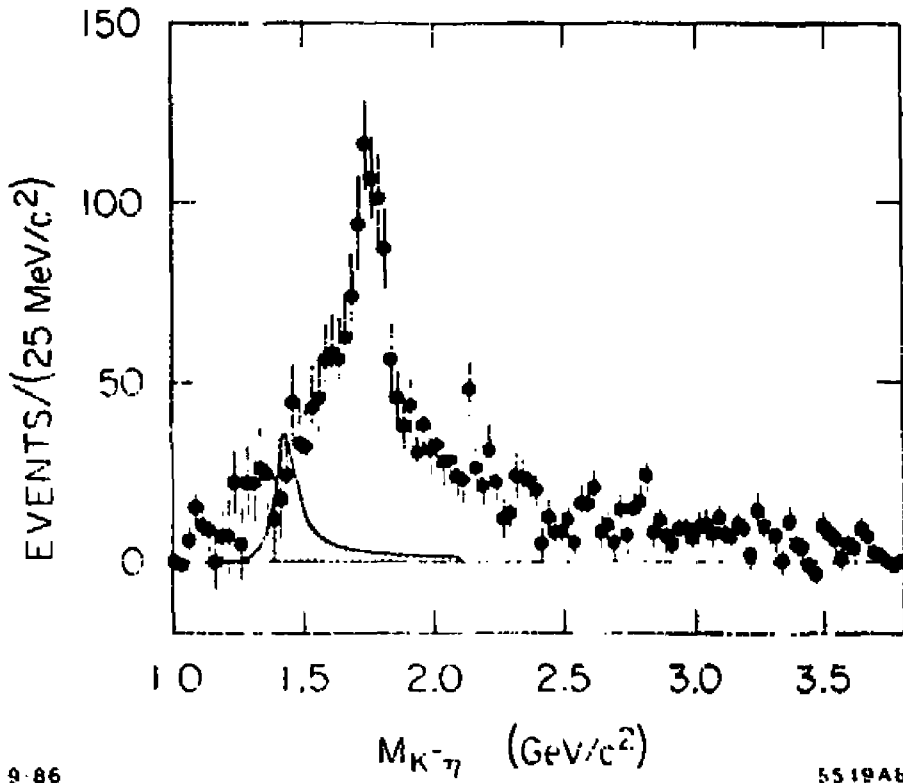
FIG 18 The background subtracted $K^-\eta$ invariant mass distribution after N^* and Y^* cuts. The shaded curve shows the signal expected for a $K^*(1430) \to K\eta$ branching ratio of 0.5%

5⁻K*₅(2380)

4⁺K*₄(2060)

2⁺K*₂(1970)
0⁺K*₀(1950)

3⁻K*₃(1780)
1⁻K* (1790)

2⁺K*₂(1430)
1⁻K*(1410)
1⁺K₁(1400)
0⁺K*₀(1350)

—— π emission
········· ρ emission
––– η emission

1⁻K*(892)

0⁻K(494)

1-87

6848A19
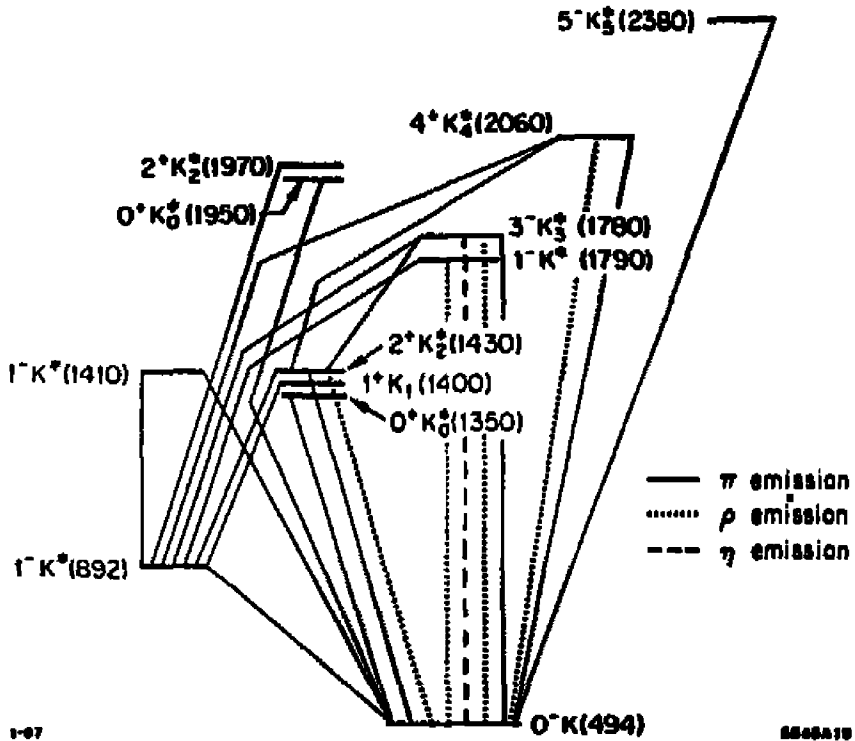
FIG. 19. Level diagram summarizing strange meson states and transitions observed in this experiment.
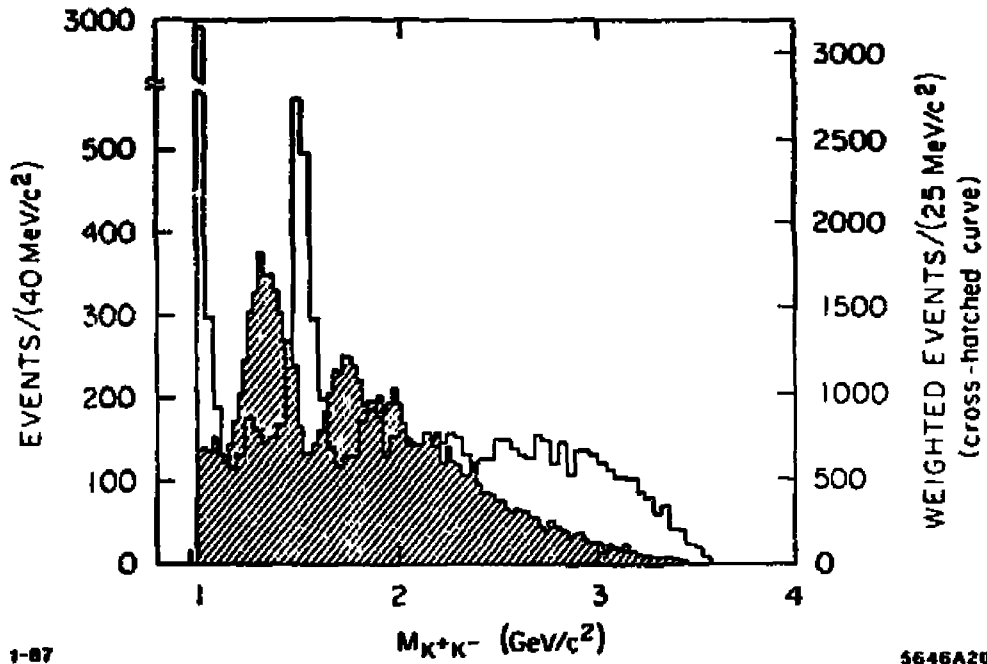
FIG. 20. Comparison of the K^-K^+ final state produced in the reaction $K^-p \rightarrow K^-K^+\Lambda$ from this experiment with the reaction $\pi^-p \rightarrow K^-K^+n$ from Ref. 9.
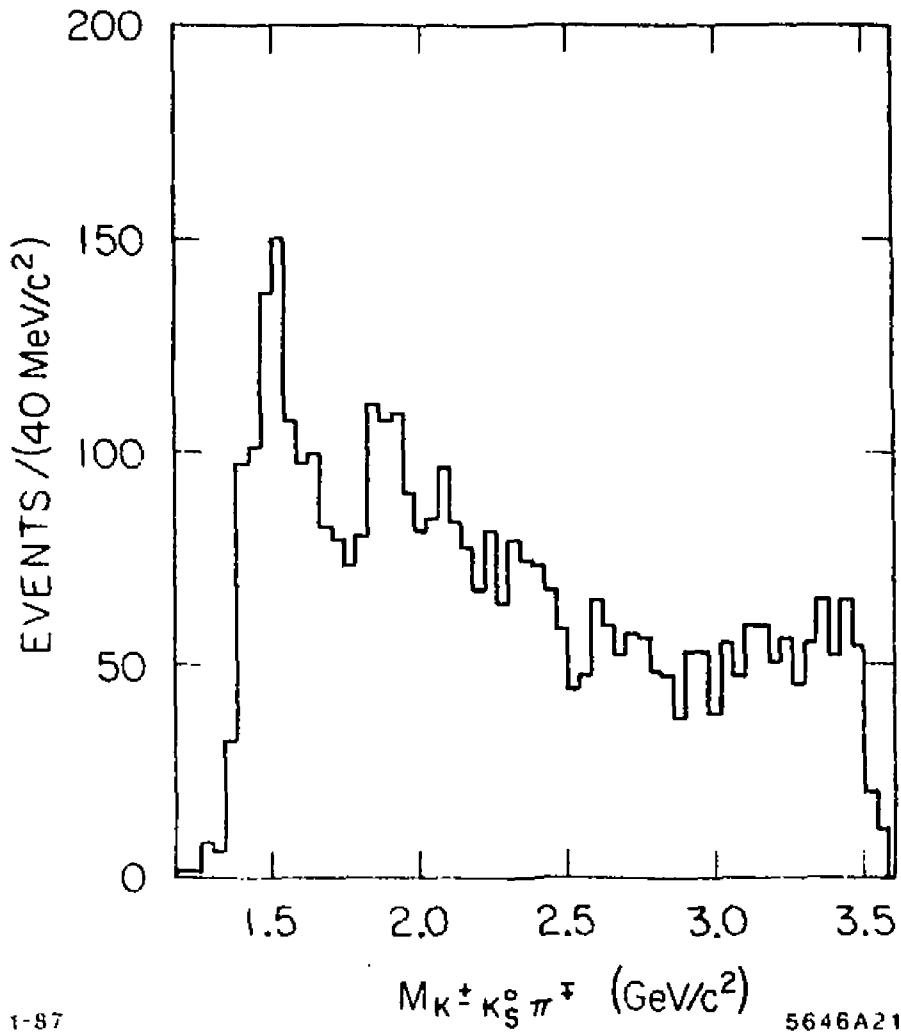
FIG. 21. The summed $K_S^o K^\pm \pi^\mp$ invariant mass spectrum for masses between threshold and 3.6 GeV/c².
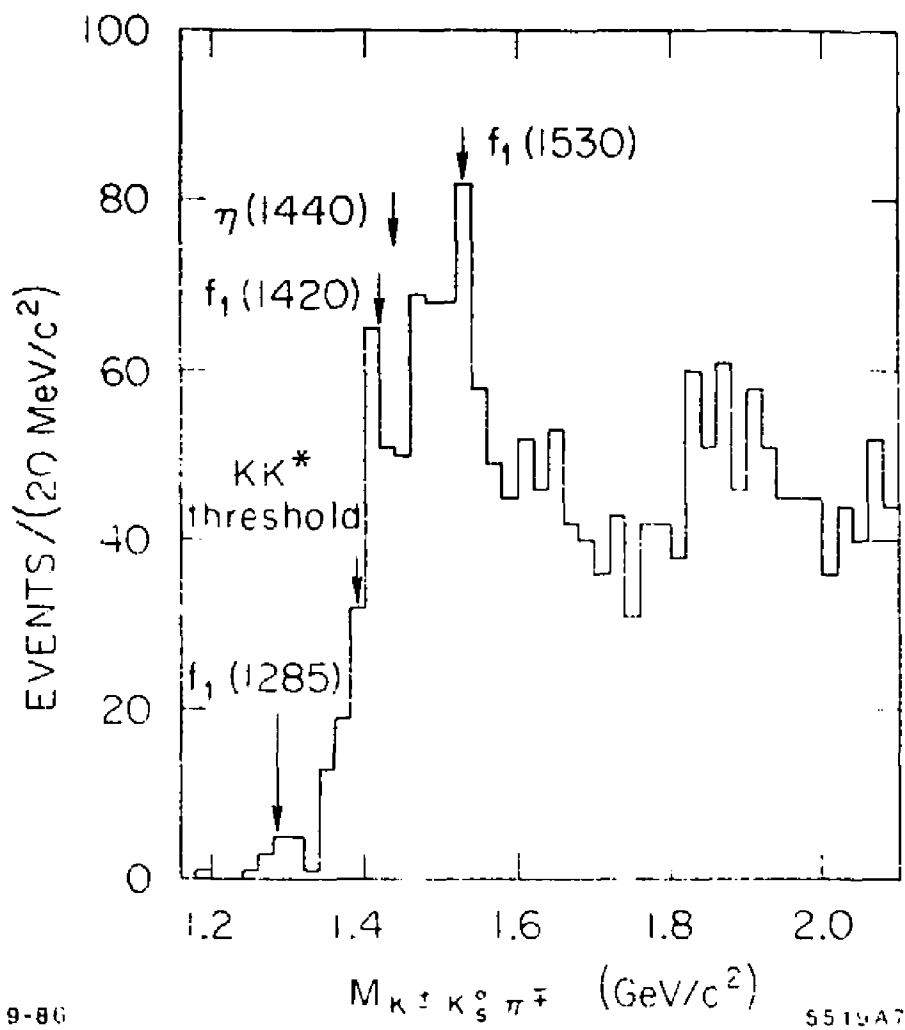
FIG. 22. The summed $K_s^0 K^\pm \pi^\mp$ invariant mass spectrum in the mass region below 2.1 GeV/c^2 in 20 MeV/c^2 bins
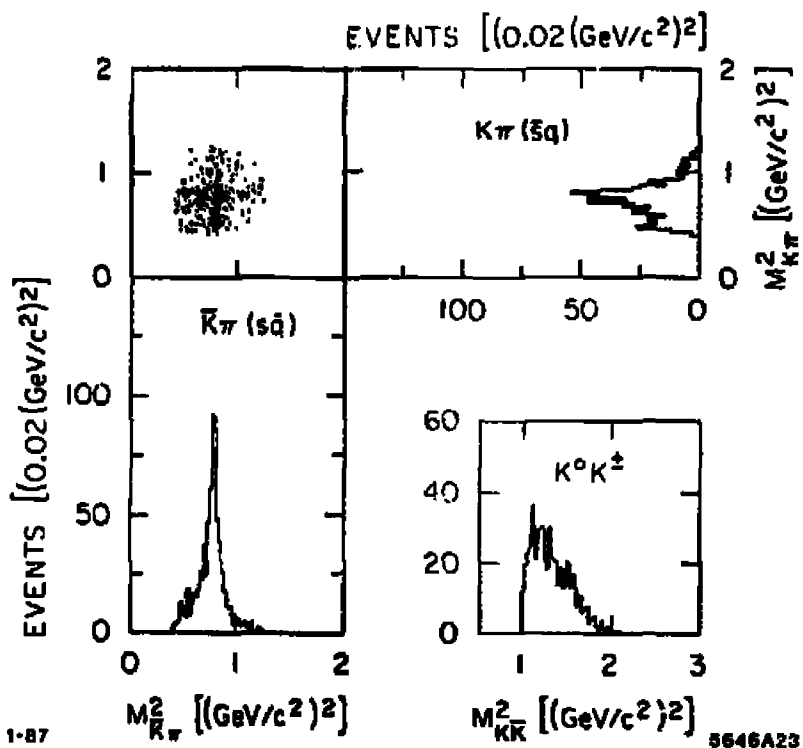
FIG. 23. Dalitz plot for the summed $K_s^0 K^{\pm} \pi^{\mp}$ final states for the mass region $1.40 \leq M_{KK\pi} \leq 1.64$ GeV/c^2. Also shown are projections for the strangeness ± 1 $K \pi$ isobars and the $\delta(K\bar{K})$ isobar.
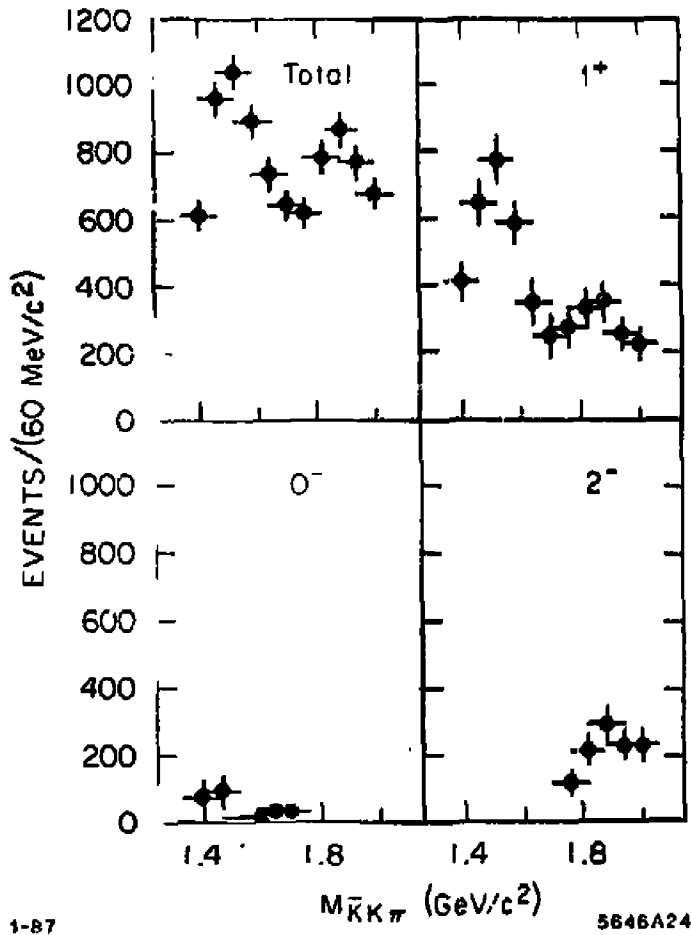
FIG. 24. The spin-parity intensity distributions required to describe the $K^0_s K^{\pm} \pi^{\mp}$ channels below 1.76 GeV/c^2. All partial waves of the same J^P are summed coherently.
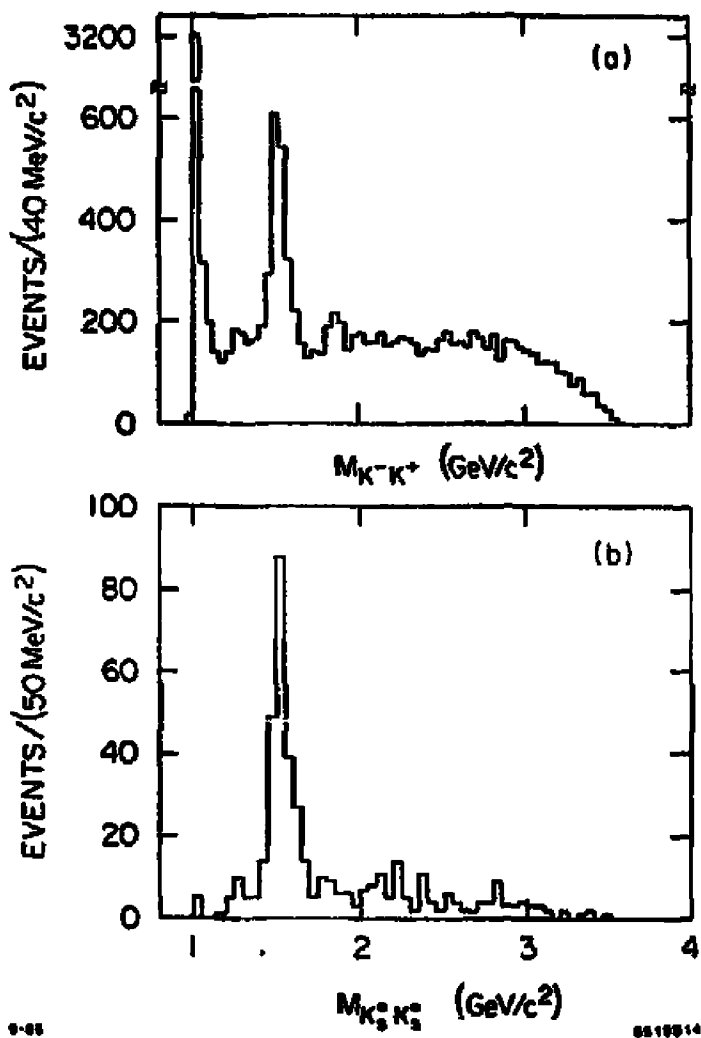
FIG. 25. The $K\bar{K}$ invariant mass spectrum for; (a) the reaction $K^-p \rightarrow K^-K^+\Lambda$; and b) the reaction $K^-p \rightarrow K_s^0 K_s^0 \Lambda$.
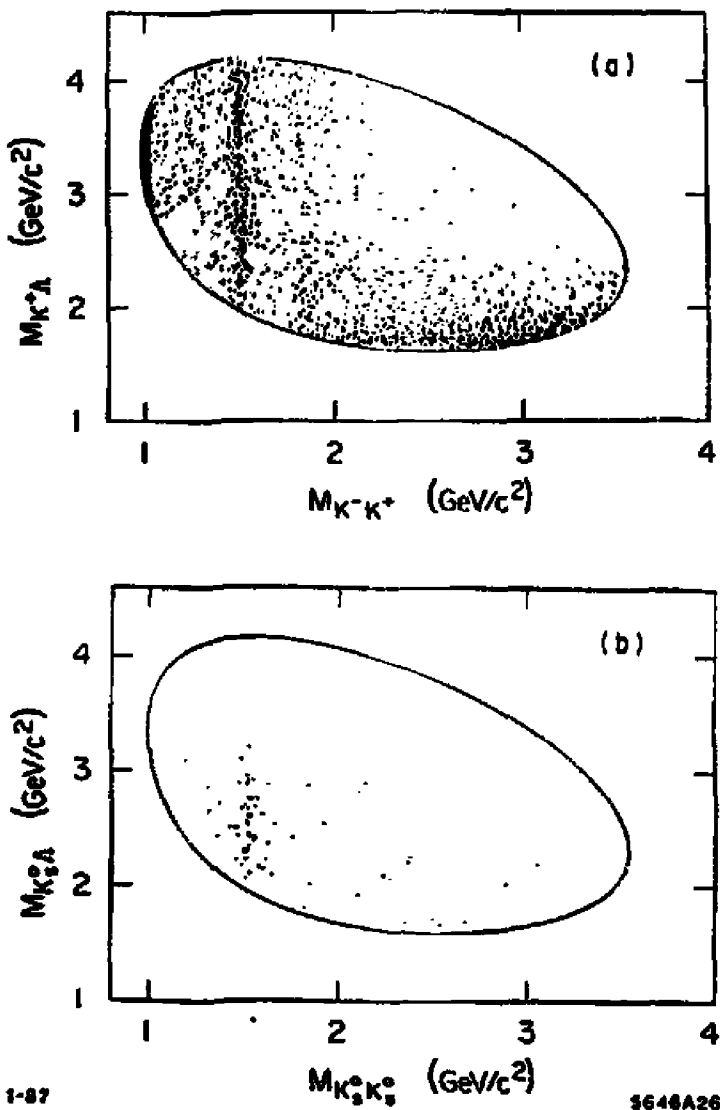
FIG. 26. Dalitz plots for a) the reaction $K^-p \rightarrow K^-K^+\Lambda$; b) the reaction $K^-p \rightarrow K^0_s K^0_s \Lambda$.
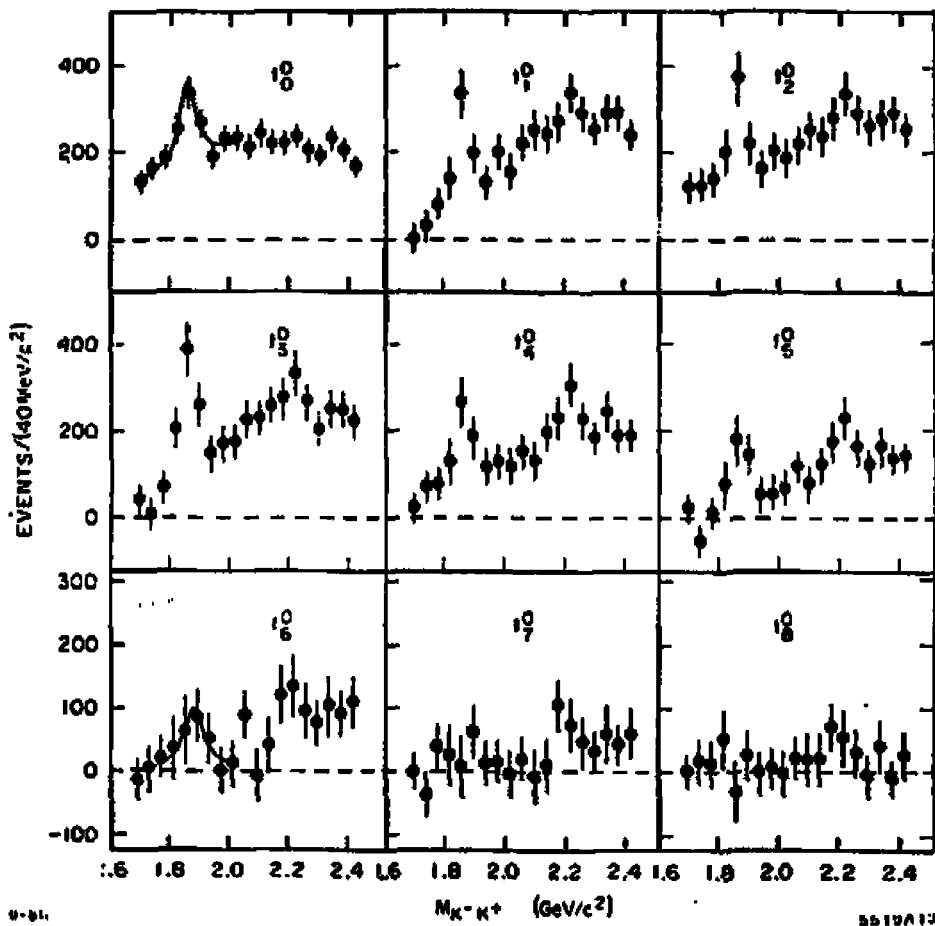
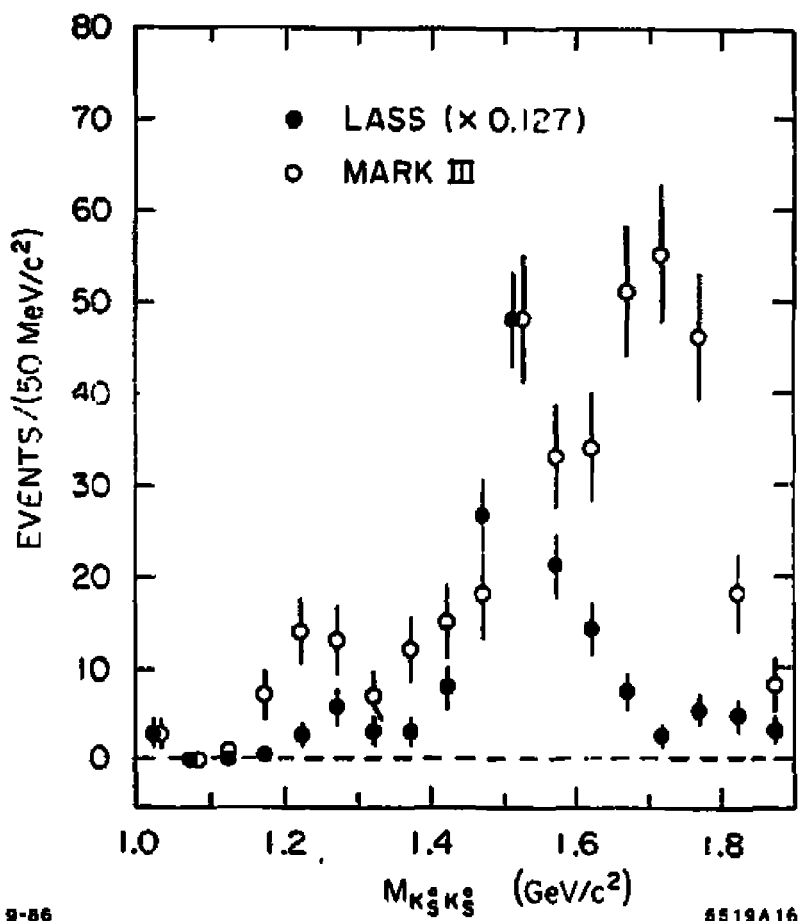FIG. 27. The unnormalized $K^-K^+ M = 0$ moments from threshold to 2.44 GeV/c^2.

EVENTS/(50 MeV/c^2)

80

70 ● LASS (× 0.127)

60 ○ MARK III

50

40

30

20

10

0

1.0   1.2   1.4   1.6   1.8
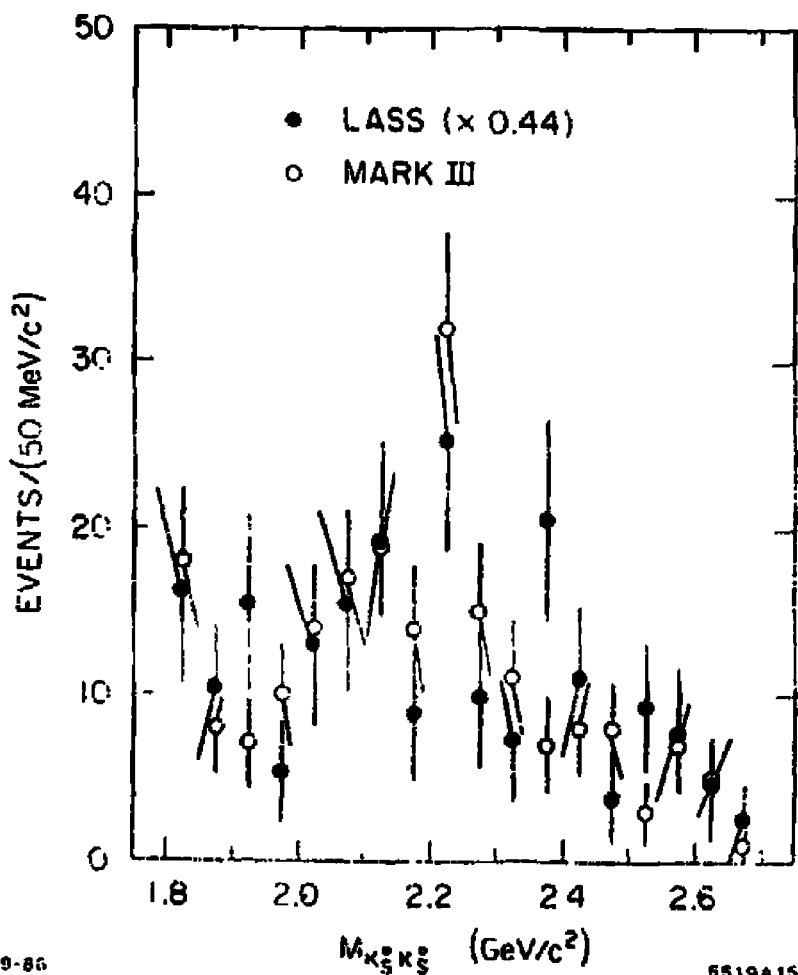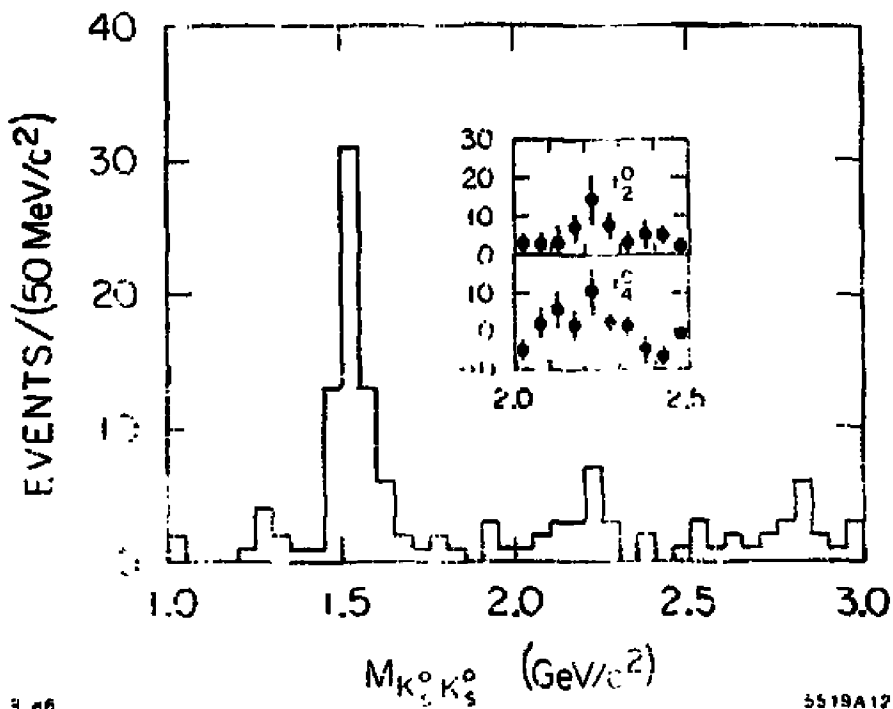
$M_{K_S^0 K_S^0}$ (GeV/c^2)

8519A16

FIG. 28. The acceptance corrected $K_s^0 K_s^0$ invariant mass distribution produced in this experiment from threshold to 1.9 GeV/c^2 compared with the same final state produced in radiative J/ψ decay as seen in the MARK III (Ref. 12).

FIG. 29. The acceptance corrected $K_S^0 K_S^0$ invariant mass distribution produced in this experiment in the region $1.8 \leq M_{K\bar{K}} \leq 2.7$ GeV/c^2 compared with the same final state produced in radiative J/ψ decay as seen by the MARK III (Ref. 12).

FIG. 30. The $K_S^0 K_S^0$ invariant mass spectrum for events with $\cos\theta_{GJ} > 0.85$. Inset are the $L = 2$ and $L = 4$, $M = 0$ moments in the 2.2 GeV/c^2 region. Moments with $L > 4$ are consistent with 0.